

# JGR Solid Earth

## RESEARCH ARTICLE

10.1029/2021JB023001

# Are Creep Events Big? Estimations of Along-Strike Rupture Lengths



### Key Points:

- Identify 2120 creep events on the central San Andreas Fault and estimate their along-strike lengths
- Creep event lengths range from sub-km to >10 km
- Existence of large events makes it likely that slip is driven by large-scale frictional weakening

### Supporting Information:

Supporting Information may be found in the online version of this article.

### Correspondence to:

D. B. Gittins,  
[daniel.gittins@earth.ox.ac.uk](mailto:daniel.gittins@earth.ox.ac.uk)

### Citation:

Gittins, D. B., & Hawthorne, J. C. (2022). Are creep events big? Estimations of along-strike rupture lengths. *Journal of Geophysical Research: Solid Earth*, 127, e2021JB023001. <https://doi.org/10.1029/2021JB023001>

Received 25 AUG 2021

Accepted 29 DEC 2021

Daniel B. Gittins<sup>1</sup>  and Jessica C. Hawthorne<sup>1</sup> 

<sup>1</sup>Department of Earth Sciences, University of Oxford, Oxford, UK

**Abstract** Segments of many faults are observed to slip aseismically at the surface. On the central segment of the San Andreas Fault, aseismic slip accumulates largely in creep events: few mm bursts of slip which occur every few weeks to months. But even though we have observed creep events worldwide since the 1960s, we still do not know how big most events are or which forces drive them. To address this uncertainty, we systematically identify creep events along the central San Andreas Fault and determine their along-strike rupture extents. We first use cross-correlation and visual inspection to identify events at individual creepmeters. With data from 18 USGS creepmeters, we identify 2120 records of creep events between 1985 and 2020. We then search for slip that is closely timed across multiple creepmeters. We identify 306 instances of closely timed slip, which could indicate 306 creep events that rupture multiple creepmeter locations. Through visual inspection and statistical analysis of timing, we identify a variety of creep event types, including single-creepmeter events, small (<2 km) events, medium-sized (3–6 km) events, large (>10 km) events, and events that rupture multiple fault strands. The existence of many large (>few-km) events suggests that creep events are not produced by small, rainfall-associated perturbations; they are more likely driven by complex or heterogeneous frictional weakening and they may provide a window into the dynamics of a larger scale slip on the San Andreas Fault.

**Plain Language Summary** The San Andreas Fault, CA, slips at the surface between San Juan Bautista and Cholame. This slip accumulates slowly or in bursts, known as creep events. Despite observations of creep events since 1966, we still do not know how large they are or what causes them to occur. Here, we determine the length of creep events as this helps us understand more about how these events are created. If creep events are small, they may be caused by rainfall; however, if they are large, then they are likely self-driven. Using 18 USGS creepmeters, we identify the timing of creep events and determine their length. Between 1985 and 2020 we have identified 2,120 creep events, some of which are recorded at multiple creepmeters, allowing us to determine their along strike-length. We identify five size ranges of our creep events: isolated events, small (<2 km) events, medium-sized (3–6 km) events, large events (>10 km), and events that occur on multiple fault strands events. These larger events are difficult to explain using conventional frictional theory and do not appear to result from rainfall. Therefore, understanding these events is important for determining the process that creates aseismic creep on faults.

## 1. Introduction

Some faults have been observed to creep at the surface since at least the 1960s. Detailed observations of creep were made following the 1966 Parkfield, CA earthquake and the 1968 Coachella Valley, CA earthquake (Bilham & Castillo, 2020; Titus, 2006). Since then, creep has been observed on many additional faults, including the San Andreas, Calaveras, and Hayward Faults in California (Evans et al., 1981; Lienkaemper et al., 2012; Steinbrugge et al., 1960); the North Anatolian Fault in Turkey (Ambraseys, 1970; Bilham et al., 2016); the Philippines Fault on the Island of Leyte (Duquesnoy et al., 1994); the Chihshang Fault, Taiwan (Lee et al., 2005; Thomas et al., 2014); and the Charman Fault, Pakistan (Fattahi & Amelung, 2016).

Here, we focus on the central creeping section of the San Andreas Fault in California. This 175 km-long segment between San Juan Bautista (XSJ) and Cholame (Figure 1) accumulates most of its slip aseismically (Titus et al., 2011). Two >100-km-long locked sections bound the creeping section. The locked section to the north of XSJ last ruptured in the 1906  $M_w$  7.9 San Francisco and 1989  $M_w$  6.9 Loma Prieta earthquakes, while the southern locked section south of Cholame last ruptured in the 1857  $M_w$  7.9 Fort Tejon earthquake (Ryder & Bürgmann, 2008; Titus et al., 2011). Smaller ( $M \approx 6$ ) earthquakes also occur near the edges of the creeping section

© 2022. The Authors.

This is an open access article under the terms of the [Creative Commons Attribution License](https://creativecommons.org/licenses/by/4.0/), which permits use, distribution and reproduction in any medium, provided the original work is properly cited.

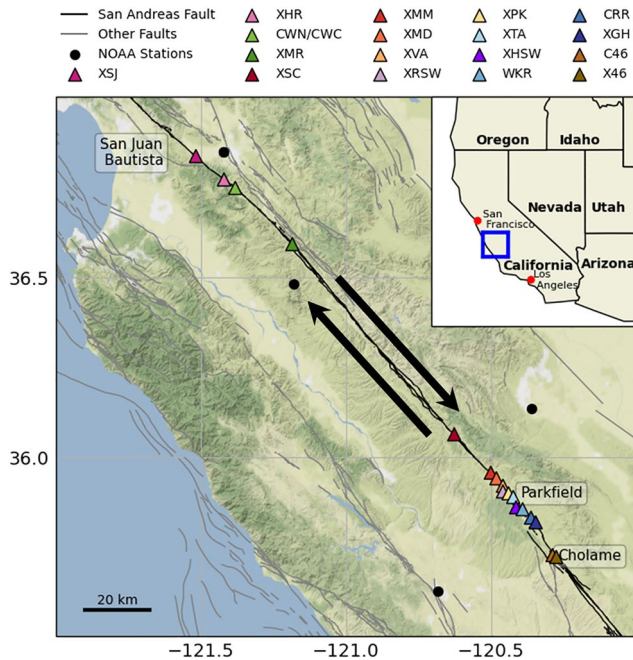


**Figure 1.** Map of the creeping section of the central San Andreas Fault (black) and other faults in central California (gray). The creepmeters are shown as colored triangles. NOAA stations are shown as black circles. Faults plotted are from the USGS/CGS Quaternary faults and folds database (<https://www.usgs.gov/natural-hazards/earthquake-hazards/faults>).

(Langbein et al., 2005). Yet, no major ( $M \geq 7$ ) earthquake has ever been reported within this 175-km-long region (Topozada et al., 2002).

But the long-term aseismic creep rate does vary along strike. The slip rate in the shallow portion of the fault decreases from 30 to 33  $\text{mmyr}^{-1}$  near the center to 10  $\text{mmyr}^{-1}$  near Parkfield and Cholame (Jolivet et al., 2015; Ryder & Bürgmann, 2008; Titus, 2006; Titus et al., 2011). Many spatial and temporal variations of creep are well recorded along the San Andreas Fault's creeping section. Following the 1966 Parkfield earthquake, the region was heavily instrumented with creepmeters (e.g., Schulz, 1989), alignment arrays (e.g., Lienkaemper, 2006), GPS (e.g., Titus et al., 2011), trilateration networks (e.g., Lisowski & Prescott, 1981), and strainmeters (e.g., Gladwin et al., 1994).

The instrumental data revealed that creep on the central San Andreas Fault and other faults does not accumulate at a steady rate (Jolivet et al., 2013; Linde et al., 1996; Roeloffs, 2001; Rousset et al., 2016, 2019). On the central San Andreas Fault, creep accumulates mostly in small bursts of accelerated slip known as creep events (Figure 2). These creep events appear small and repetitive. They display mm to cm of slip, last hours to days, and recur at intervals of weeks to months (Gladwin et al., 1994; Schulz, 1989; Wei et al., 2013; Wesson, 1988). There are larger creep events as well, with durations of weeks to years, but these larger events either accommodate small fractions of the surface slip or contain smaller bursts within them (e.g., Linde et al., 1996; Roeloffs, 2001). It appears that the small repetitive creep events play a dominant role in accommodating surface slip. But even though we know that small creep events are abundant and accommodate more surface slip on the 175-km creeping section, we do not know which fault zone processes cause creep events. We do not even know how *spatially* large most creep events are: how far the ruptures extend along strike or along depth.

We do not know the spatial extent of most creep events because previous work has focused on a handful of larger events or repeated events at an individual creepmeter (e.g., Bilham & Behr, 1992; Evans et al., 1981; Gladwin et al., 1994; Gouly & Gilman, 1978; King et al., 1973; King, 2019; Mchugh & Johnston, 1976; Mortensen et al., 1977; Nason & Weertman, 1973; Slater & Burford, 1979). Furthermore, slip at an individual creepmeter tells us only about the slip at a particular location; it does not tell how much of the fault is slipping. Previous estimates of the size of creep events vary widely and are summarized in Table 1. Some analyses have implied creep events are just short (640 m), shallow ruptures (30–510 m depth) (Figure 3a) (e.g., Gladwin et al., 1994; Gouly & Gilman, 1978; Mortensen et al., 1977) or long (6.6 km), shallow ruptures (510–1400 m depth) (Figure 3b) (e.g., Evans et al., 1981; Mchugh & Johnston, 1976). However, other evidence implies that creep events could be long and deep, rupturing to depths of 4 km, perhaps all the way to the seismogenic zone (Figure 3c) (e.g., Bilham et al., 2016; King, 2019; King et al., 1973; Mortensen et al., 1977).

It is essential to know how large creep events are if we are to understand why they happen: to know what is happening in the fault zone that allows these episodic slow events. For instance, if creep events are small and shallow, one might imagine that the creeping San Andreas Fault is slip rate-strengthening, with a stable frictional rheology. Creep events could occur on a nominally stable fault if the fault receives some "kicks" in stress or pore pressure, perhaps from the stress perturbations by rainfall and atmospheric pressure (Kanu & Johnson, 2011; Helmstetter & Shaw, 2009). However, the "kick" hypothesis only seems plausible if creep events are shallow, occurring in a region with low normal stress that provides only modest resistance to acceleration. If creep events are large and deep, it seems more plausible to imagine that they are self-driven: driven by local frictional weakening. However, self-driven creep events are challenging to explain with conventional rate-strengthening or rate-weakening rheologies. To display the episodic but aseismic slip seen in creep events, a fault may require particularly sized patches of rate-weakening material (e.g., Liu & Rice, 2005; Luo & Ampuero, 2018; Rubin, 2008; Skarbek et al., 2012; Wei et al., 2013; Yabe & Ide, 2017) or a more complex fault zone process such as shear-induced dilatancy (e.g., Iverson, 2005; Leeman et al., 2018; Segall et al., 2010; Segall & Rice, 1995; Shibazaki & Iio, 2003).

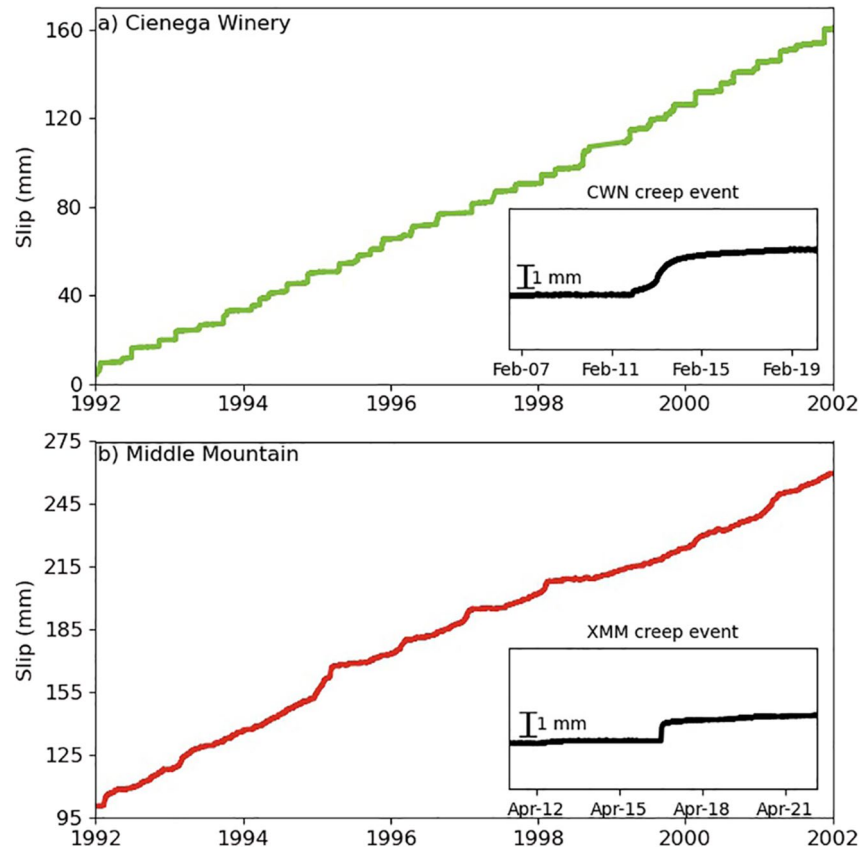


**Figure 2.** 10 years of slip at two creepmeter locations that show creep events of different character: (a) Cienega Winery (CWN), showing a multistep creep event and (b) Middle Mountain (XMM), showing a single step creep event.

The different creep event sizes presented in Figure 3 also have different implications for the release of the strain that accumulates along the central creeping section. Geodetic observations suggest that the central San Andreas Fault is slipping slower than the long-term slip rate, accumulating a moment deficit (Maurer & Johnson, 2014; Michel et al., 2018; Ryder & Bürgmann, 2008). That moment deficit could be accommodated by a  $M_w$  5.2–7.2 earthquake occurring every 150 years, on average (Maurer & Johnson, 2014; Michel et al., 2018; Ryder & Bürgmann, 2008). Or the moment deficit could be accommodated by occasional bursts of creep events (e.g.,

**Table 1**  
*Some Previous Estimates of the Spatial Extent of Creep Events*

Instrument	Location	Along-strike length	Depth extent	Scenario	Reference
Tiltmeter	SAF near Hollister	couple of km	>0.5–2 km	b	Mchugh and Johnston (1976)
Strainmeter	SAF near San Juan Bautista	few km	200–500 m	a	Gladwin et al. (1994)
Strainmeter	Cholame Valley	640 m	30–510 m	a	Gouly and Gilman (1978)
Strainmeter	Calaveras Fault	6.6 km	510–1400 m	b	Evans et al. (1981)
Kinematic modeling	Calaveras Fault	5.6 km	2.8 km	c	King et al. (1973); King (2019)
Multiwavelength distance measuring	Calaveras Fault	—	approx 1 km	b	Slater and Burford (1979)
Tiltmeter, strainmeter, and water-level fluctuations	Cienega Winery	0.8 m–4 km	0.4–2 km	a and c	Mortensen et al. (1977)
Strainmeters and creepmeters	NAF near Ismetpasa	—	4 km	c	Bilham et al. (2016)
Dislocation modeling	—	0.1–5 km	—	—	Nason and Weertman (1973)
Creepmeters	Superstition Hills	—	0.3–3 km	a, b, and c	Bilham and Behr (1992)
Creepmeters	SAF near Melendy Ranch	1.2 km	—	—	(Burford, 1977)

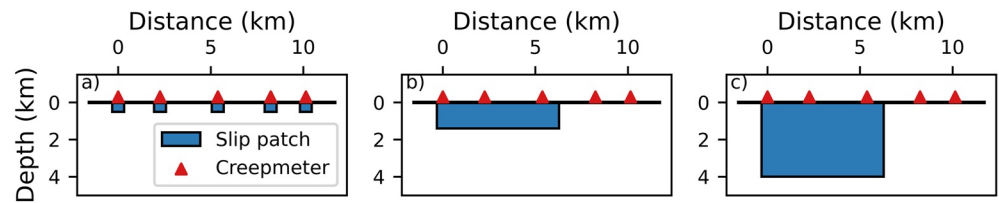


**Figure 3.** Three creep event size scenarios. (a) Short, shallow ruptures. (b) Long, shallow ruptures. (c) Long, deep ruptures.

Khoshmanesh & Shirzaei, 2018b). A moment deficit that requires a  $M_w$  6.2 earthquake per 150 years could be accommodated by a burst of 200 1 mm creep events that are 10 km along strike and 4 km deep occurring every 30 years. But if creep events are much smaller and shallower, say 5 km long and 1 km deep, the observed moment deficit could be accommodated only by a burst of 800 1 mm creep events every 15 years.

In this study, we thus aim to take an important next step in unraveling the origin and role of creep events in the slip dynamics of the creeping section. We aim to determine the typical along-strike extent of creep events on the central San Andreas Fault. We first systematically identify creep events within the remarkable, decades-long USGS creepmeter record. Then, we compare records from multiple creepmeters to characterize the ruptures' along-strike extents and determine if they are small, localized phenomena or large, segment-rupturing events.

## 2. Creepmeters and Creep Events

We use data from 18 USGS creepmeters along the creeping section of the San Andreas Fault (Figure 1) to investigate the along-strike length of creep events. Each creepmeter operated for at least nine years between 1985–2020. All creepmeters have sampling interval of 10-min except for Melendy Ranch (XMR), which was upgraded to 1-min sampling on 6 September 2018 by the USGS and R. Bilham. Detailed descriptions of each creepmeter and its site location can be found in Schulz (1989).

The creep events we analyze are mostly well recorded. They appear in the data as accelerated bursts of slip (Figure 2). Typical creep events last from hours to days and slip on the order of less than a millimeter to several millimeters (Bilham et al., 2004; Wesson, 1988). Creep events may be simple and have a sharp onset (Figure 2b) or have multiple steps (Figure 2a) that could reflect a migrating slip location (Bilham & Behr, 1992; Gladwin et al., 1994; Schulz, 1989; Wesson, 1988). Creep events may also have a smaller initial step or increased slip rate (sometimes referred to as preamble) preceding the main slip period (Bilham et al., 2004; Wesson, 1988). Occasionally, there is a slight plateau between the first and second phases of slip in multistep events, where the slip rate is above the background rate but slower than both steps on either side. The length of this plateau is not the same between events, so it is unlikely to be an instrumental artifact (Gladwin et al., 1994). Despite all the possible variations in creep events, whether single or multi-step, sharp or gradual onset, creep events appear to be self-similar at each creepmeter. However, creep events do not have a similar form across creepmeters, giving each creepmeter its own characteristic creep event (Wesson, 1988).

Creep events are not the only signal present in the creepmeter data. There are also many steps in the data. Some steps result from small nearby earthquakes, while others arise because of friction within the creepmeter instrumentation (Bilham & Castillo, 2020). These steps are usually distinguishable from creep events because they occur abruptly, while creep events typically have a longer duration and asymptotically approach a lower slip rate (Figure S1 in Supporting Information S1).

## 3. Identifying Creep Events at Individual Creepmeters

In order to constrain creep events' spatial extent and timing, we first needed to find the events in the data. The creep events we are interested in are readily identifiable via visual inspection. Through visual inspection alone, it is possible to characterize the slip and duration of creep events and develop an understanding of the typical shape that a creep event has at each creepmeter. Yet despite the ease of which detecting creepmeters manually can be achieved, visually examining decades of creepmeter records would be time-consuming. So we identified the

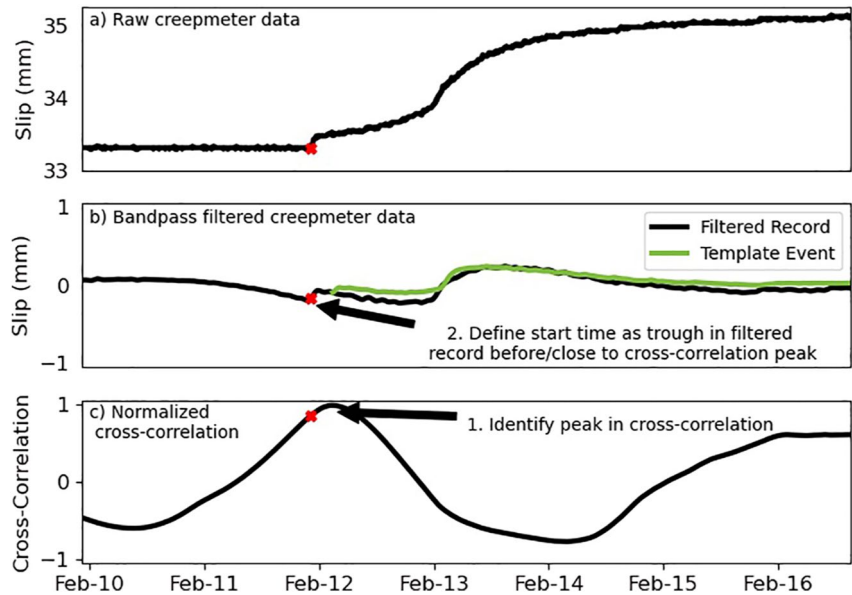


**Figure 4.** Processing stages of the automated detection. (a) Raw creepmeter data from Cienega Winery (CWN) showing a creep event on 11 February 1994. (b) The same creep event band-pass filtered between 2 hr and 5 days (black line), along with the template creep event (green line). The template has been aligned with the data according to the peak of the cross-correlation time series shown in panel (c). The red cross in all panels indicates the estimated creep event start time, taken as the time of the trough in the filtered data in panel (b).

creep events at each creepmeter using an automated approach to obtain initial potential detections. Then we used visual inspection to refine the catalog.

The aim of this automated detection was to find the creep events that we already knew were there as well as those at other creepmeters that at the time we had not examined. Before beginning the process of building the automated detection, we manually picked creep events at XSJ, Harris Ranch (XHR), and Cienega Winery (CWN). We tested our automated detection against these manual picks in order to ensure that our detection was not missing events that we had observed by inspecting the creep record by eye. We find that for these creepmeters we were able to detect >90% of creep events detected through manual inspection, only missing either very small events or events that have a more surge-like shape, which lasted on the order of months and had ambiguous onsets and end times. These surge-like creep events are much less frequent than the step-like creep events that make up the vast majority of the creep record.

### 3.1. Automated Detections

A full in-depth description of our automated detections is presented in Text S1 in Supporting Information S1. Here, we detail the main processing steps undertaken by our detection scheme.

We began by identifying times of potential creep events: times when the creepmeter record is similar to a template creep event and when there is a significant slip.

For this analysis, we first prepared the data. We interpolated the creepmeter record to ensure that the data were spaced evenly at 10-min intervals, removed a long-term trend, and band-pass filtered to focus on variations between 2 hr and 5 days: the dominant periods of the creep events (Bilham et al., 2004; Gladwin et al., 1994; Westson, 1988). The black curves in Figure 4a and 4b illustrate a creep event record before and after filtering. We then picked one template creep event for each creepmeter (green curve in Figure 4b). One creepmeter is an exception; we used two templates for the XMR creepmeter, as the data's sampling frequency increased after it was updated. We tried using different template events for detecting creep events all of which performed very similar to one another, varying only in the start time which they detected. As we eventually correct for the discrepancy in start time manually, the choice of template event for each creepmeter was less crucial as long as it was representative of the vast majority of events.

Next, we conducted a rough automated detection by cross-correlating the template creep events with the creepmeter records. The length of the time window for our cross-correlation was the length of the template event and was calculated as a sliding window. We identified peaks in the cross-correlation that exceeded a creepmeter-dependent threshold between 0.05 and 0.2, allowing only one peak per 40-min interval (Figure 4c). The thresholds for detection were set relatively low, allowing for many false positives so that we could identify creep events with shapes that varied from the template.

After identifying the potential creep events, we estimated their start times by examining the running average of the slip in hourly windows just before and after the cross-correlation peak. We identified the potential event start as the time when this hourly slip first appears significant: when it exceeds a noise-based threshold value. Then we refined the start times using a feature of the filtered creep record: a distinct trough at the start of creep events (Figure 4b). This trough has no physical meaning and is purely an artifact of the detrending and filtering processes we used. Despite this, the trough before creep events proved useful to more accurately determine the start time of creep events. We used the time of the nearest trough to the start time we had determined using hourly slip as our automated estimate of the potential creep events' start times (red cross in Figure 4).

To estimate the potential creep events' end times, we examined the running average of the slip in overlapping daily windows following the start time. End times were estimated as the first time after the event began, where this daily slip fell below a noise-based threshold.

Once we had end time estimates, we could calculate the slip in each potential creep event. We subtracted the slip at the start time from the end time. This simple difference provides the best estimate of the slip in the identified time period, given that the noise in the creepmeter record has a random walk character at periods longer than 1 hr (e.g., Langbein et al., 1993; Langbein and Johnson, 1997).

The slip estimates provided a useful way of removing tiny events, most of which result from instrumental resolution or friction within the creepmeters. We removed detections when they had slip less than 1% of the median slip from the largest 10% of creep event detections at each creepmeter.

In our last automated step, we merged events as necessary. Some creep events include multiple accelerations and those can be detected as multiple creep events. We merged the detections if the start and end times of two potential creep events were the same or overlapped. After completing this step, our catalog of potential creep events includes 15,180 events.

Finally, we visually inspected all of the potential creep events to ensure no false positives are carried forward into further work. We manually corrected each start time based on a visual inspection of the data.

### 3.2. Results

With our automated and manual analysis, we identified 2,120 creep events at 18 creepmeters. This event catalog is provided in Supplementary Section 2. Figure 5 shows some of the patterns evident in this catalog: the number of events at each creepmeter, as well as the events' median slip and duration. There is an anti-correlation between the number of creep events at each creepmeter (Figure 5a) and the slip (Figure 5b) and duration (Figure 5c) of those events. These properties are plotted against one another in Figure S2 in Supporting Information S1. This summary confirms our inferences from visually examining the record: that some fault sections slip in numerous creep events, each with small slip (e.g., Middle Mountain, XMM [Figure 2b]), while others slip less frequently, in creep events with large slip (e.g., CWN [Figure 2a]). Despite the varying sizes and number of creep events, most creepmeters see over 50% of their total slip accommodated in creep events (Figure 5d). The exception to this are creepmeters with a surge-like slip that is not detected as a creep event under our detection scheme or creepmeters that suffer from a large amount of left-lateral slip, meaning that the percentage of slip accommodated in creep events is less clear. These percentages show that creep events play an important role in accommodating fault slip at the surface. To remove some of the bias created by the available record we have also plotted median slip per event normalized by the median recurrence interval (Figure 5e). This proxy for slip rate shows a similar pattern to the percentage of slip accommodated by creep events in Figure 5d. The total slip accommodated in creep events at the surface does not account for the total slip observed at depth along the creeping section as the values of median slip per median recurrence interval (Figure 5e) are lower than 30–33  $\text{mmyr}^{-1}$  leading to a slip deficit (Maurer & Johnson, 2014; Michel et al., 2018; Ryder & Bürgmann, 2008).

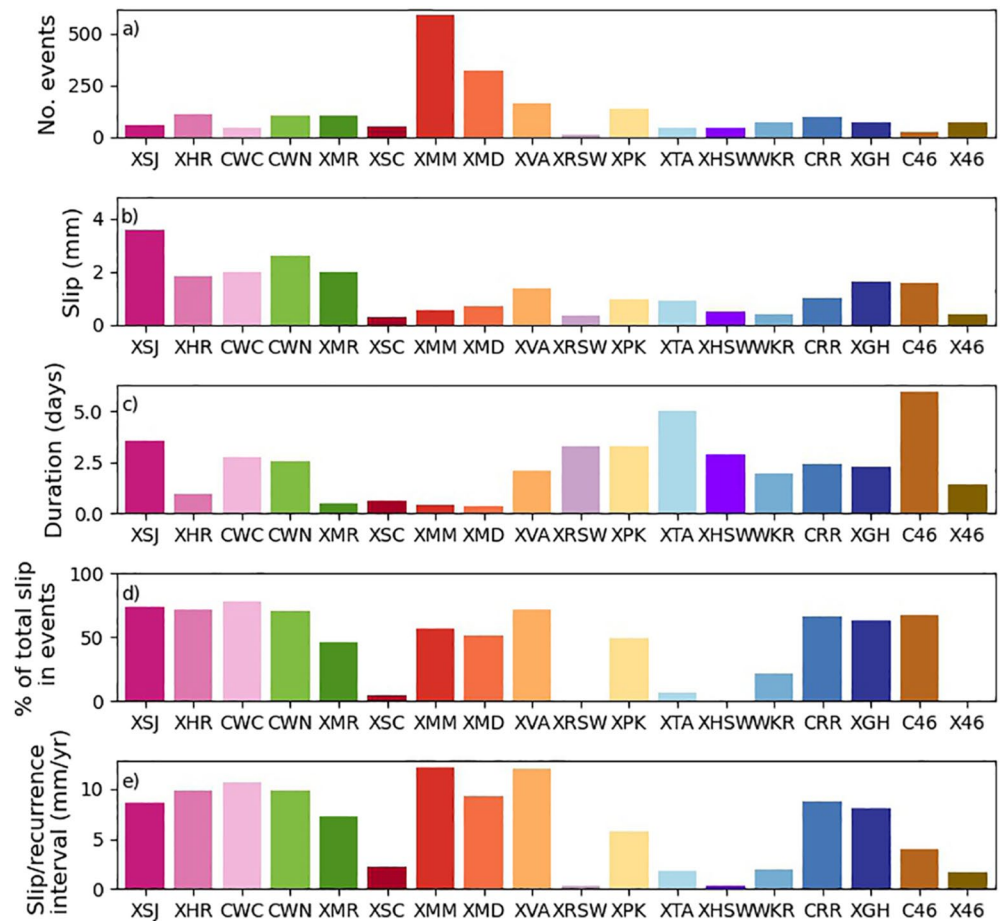


**Figure 5.** Properties of the creep events at each creepmeter. (a) Number of detected events. (b) Median creep event slip. (c) Median creep event duration. (d) Percentage of total fault slip accommodated in creep events. Note Roberson Southwest (XRSW), Hearst Southwest (XHSW), and X46 do not have values. This is due to a large amount of left-lateral slip making calculating the total amount of slip for these creepmeters not easily quantifiable. (e) Median slip divided by median recurrence interval.

We find that creep events along the San Andreas Fault have a recurrence time of weeks to months and vary along the fault (Figure S3 in Supporting Information S1). Furthermore, the creepmeters with fewer, larger creep events appear to have longer recurrence intervals than those with more frequent smaller events. The frequency of creep events is not consistent through time and is affected by seismicity. For instance, the recurrence interval of creep events at creepmeters affected by the 2004 Parkfield Earthquake (Slacks Canyon [XSC]–Gold Hill [XGH]) is shorter in the 10 years after the earthquake than in the 10 years before it (Figure S4 in Supporting Information S1).

Using our creep event catalog, we have produced a booklet (Section 3 in Supporting Information S1) displaying all the creep events we observe and the creep recorded on other creepmeters at the time of the event. This booklet was useful in identifying creep events that may rupture the surface at more than one creepmeter (Section 4.3).

#### 4. Identifying Correlated Events Between Creepmeters

An initial visual analysis of the creep event records suggested that some of the creep events span relatively long distances along strike (Figures S5 and S6 in Supporting Information S1). Both Figures show creep events through time, allowing for the correlation of creep events across different creepmeters. In this section, we describe how we used the closely timed event detections to determine the spatial extent of creep events. We describe how we determined the frequency of multi-creepmeter events, accounted for rainfall-induced coincidences, and visually

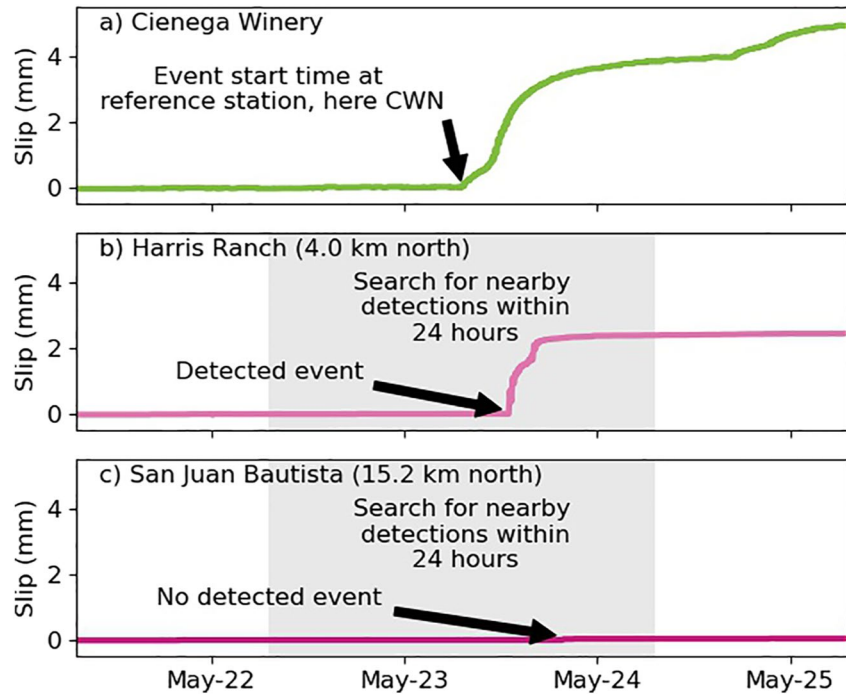


**Figure 6.** Creep records for the 21–26 May 2016 at (a) Cienega Winery (CWN), (b) Harris Ranch (XHR), and (c) San Juan Bautista (XSJ). The figure illustrates our approach to detecting closely timed events. For each event at CWN (panel a), we search for events at (b) XHR and (c) XSJ that occur within 24 hr of the CWN event (gray regions in panels b and c).

examined identified ruptures. We summarize the common creep event behaviors identified with this analysis in Section 5.

#### 4.1. Estimating the Frequency of Multi-Creepmeter Ruptures

It is clear from the records in Figure 6 that, during this period, creepmeters 4 km apart display creep events at close times, and it would seem plausible that the events result from a single, >4-km-long creep event. However, it is also possible that the closely timed events are just a coincidence or just a rare large creep event. Our next task, then, was to determine the fraction of creep events observed at one creepmeter that have a closely timed event at another.

We examined the frequency of closely timed creep events at all pairs of creepmeters. We first isolated the period in which both creepmeters were operational, excluding the period between 28 September 2004 and 1 January 2006 on southern creepmeters because this interval is affected by the 2004 *M*<sub>6</sub> Parkfield earthquake. We defined one creepmeter in each pair as the main creepmeter. For each creep event on this main creepmeter, we identified the closest event on the second creepmeter and noted the time between the two. Since creep events typically last hours to days, we were particularly interested in when the time between creep events was less than 24 hr. We calculated the percentage of creep events observed at the main creepmeter that occur within 24 hr of a creep event at the second creepmeter.

We selected 24 hr as the threshold value as it provides a balance between detecting slow propagating events and conducting robust statistics. Previously reported propagation velocities for creep event range from 960 m/day to 82.32 km/day (e.g., Evans et al., 1981; King et al., 1973; Mortensen et al., 1977). We have calculated the theoretical propagation velocities (Figure S7 in Supporting Information S1) for any event at one creepmeter that occurs within 24 hr of another event at a different creepmeter regardless of distance along the fault. We find that 60.5% of these possible propagating events have a propagation velocity within the range of those previously reported (Figure S7 in Supporting Information S1). Only 1% of these possible propagating events have a propagation velocity of less than 960 m/day. This suggests that we are only missing the very slowest propagating events. We,

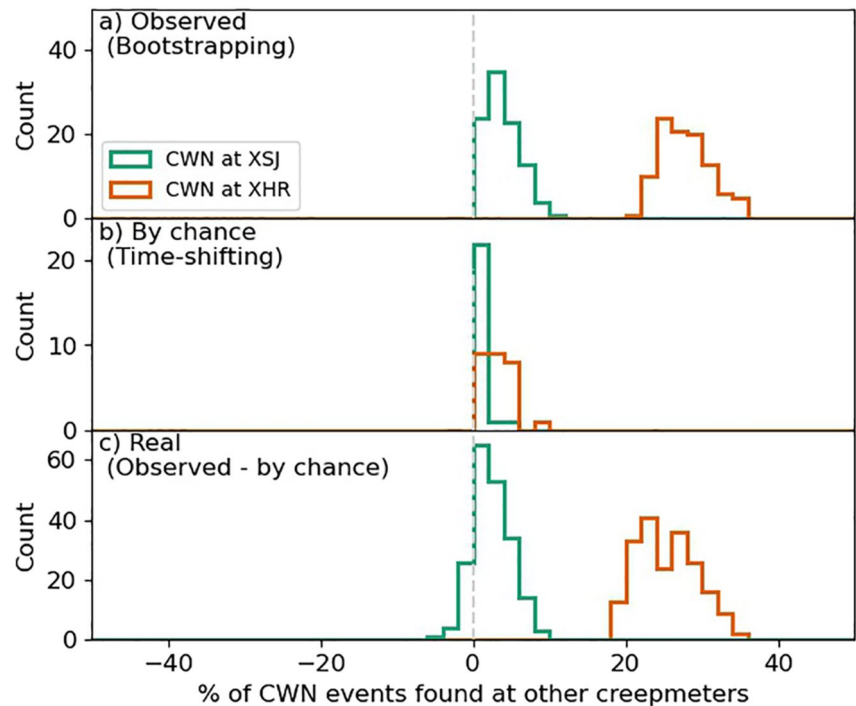


**Figure 7.** (a) Probability distributions of the percentage of Cienega Winery (CWN) creep events observed at Harris Ranch (XHR) (orange) and San Juan Bautista (XSJ) (green) within 24 hr, based on bootstrapping. (b) Probability distributions that a CWN event would coincide with an XHR or XSJ event by chance: if events were randomly timed. (c) The distributions in (a) minus the distributions in (b): probability distributions on the percentage of CWN events that observed at XHR and XSJ within 24 hr for a physical reason.

therefore, choose not to use a time window shorter than 24 hr as this reduces the possibility of detecting slower propagating events.

Using a window longer than 24 hr adds additional unwanted complexity to the statistics and interpretation. For instance, if we consider a window of 3 days before or after an event, the total time window we need to search for another event is 6 days. At these timescales, it is possible that two events have occurred at one creepmeter and both events would correlate with the target event at the main creepmeter. These double correlations are particularly troublesome in the years following the 2004 Parkfield earthquake, when the recurrence interval of creep events is reduced (Figure S4 in Supporting Information S1). Interpretation of these double correlations is also problematic. It becomes unclear whether all three of these detections are: one event that propagates back on itself, two events where one is detected at more than one creepmeter, or three separate unrelated events. For simplicity of understanding, we, therefore, chose to use a correlation window of 24 hr as this provides both a long enough window to find events that have propagation velocities in the range of those previously reported while also allowing us to conduct more robust statistics without double correlations.

Next, we calculated the uncertainty on this percentage of closely timed creep events. We bootstrapped the data and recomputed the percentage using various subsets of the creepmeter records. We divided the main creepmeter record into years, and in each recomputation, we picked the same number of years as in the original record, but with replacement, and calculated the percentage of these creep events within 24 hr of events at the second creepmeter. This bootstrapping allowed us to estimate a probability distribution on the percentage of events at the main creepmeter that occur within 24 hr of an event at the second creepmeter. The 15th to 85th percentiles of the orange histogram in Figure 7a tells us, with 70% probability, that 24.3%–31.5% of CWN events are within 24 hr of an event at XHR.

However, closely timed events are not necessarily physically meaningful; some of the XHR events could occur just before or after CWN events by chance. To determine how many events could be closely timed by chance, we redo our analysis after randomly shifting the times of creep events at the main creepmeter by 1–35 years. In each

reanalysis, we shifted all of the creep event times by the same amount, looping the times of events shifted beyond the end of the record back through the start. With this constant shift, we were able to maintain the temporal spacing and thus the recurrence statistics of the creep events. Further, we use time shifts that are multiples of 1 year to preserve the seasonality of the creep event timing. This time-shifting creates a distribution (Figure 7b) that encompasses the percentage of creep events recorded on two creepmeters by chance and unrelated.

To estimate the number of “real” closely timed events—those that are not by chance, we subtracted the by chance distribution (Figure 7b) from the bootstrapped observed distribution (Figure 7a). The probability distribution of these real closely timed events is shown in Figure 7c, in green for the CWN-XSJ pair and orange for the CWN-XHR pair. In Figure 7c, the CWN-XSJ distribution crosses 0% (vertical dashed gray line) and has a 70% confidence interval of 0%–5.1%, meaning that coincidentally timed events are likely to be unrelated. In contrast, the CWN-XHR distribution is well above 0%, with a 70% confidence interval of 21.3%–29.1%, indicating that coincidentally timed events are related.

The percentages of events for of each creepmeter pair are presented in Figures S8–S24 in Supporting Information S1. Certain pairs are discussed in more detail in Section 5.

#### 4.2. Removing Short-Term Rainfall Effects

Our results suggest that for many pairs of creepmeters, events are closely timed more often than one would expect by chance. However, these temporal coincidences do not necessarily imply that a single creep event ruptures from one creepmeter to the other; there could be two small events, one near each creepmeter (e.g., Figure 3a). These two small events could be closely timed because they both respond to atmospheric or hydrological signals.

Hydrological signals can appear in the creepmeter record on both short- and long-timescales (Bilham et al., 2004; Roeloffs, 2001; Schulz et al., 1983). The long-timescale hydrological signals are the result of seasonal variations. These seasonal variations manifest in the number of creep events that occur during the wet and dry seasons as well as the overall creep rate (Roeloffs, 2001). The long-timescale components of seasonal hydrological signals are already accounted for in our by-chance distributions, as we used only time shifts that were multiples of a year.

On short-timescales, rainfall can influence creep rate as well as creep events. Given that fault zone material of creeping faults is generally rich in clays (e.g., Kaduri et al., 2017; Moore & Lockner, 2013; Moore & Rymer, 2012, 2007), rainfall will cause the shallow fault to expand as the clay moistened and contract when dry, forcing the piers that anchor the creepmeter in place in random directions adding noise (Bilham et al., 2004). Creep events are also affected by rainfall with episodic slip induced following periods of heavy rain (Roeloffs, 2001) and retardation of slip in dryer periods (Schulz et al., 1983). Creep events that are closely timed with rainfall could be a result of the rainfall providing a “kick” to a shallow portion of the fault that has nominally stable rheology and low resistance to slip at near-surface low-stress conditions (Kanu & Johnson, 2011; Helmstetter & Shaw, 2009; Perfettini & Ampuero, 2008). As this mechanism for creep events does not represent a tectonically driven process, we need to assess to what extent these longer events are driven by rainfall.

Here, we probe the shorter-timescale influence of rainfall to interpret our results in the light of rainfall being a possible source of our longer multi-creepmeter events.

To probe the rainfall effect, we again recomputed our closely timed event percentages (Section 4.1), but with few modifications. We used rainfall records from the four NOAA weather stations to identify creep events at the main creepmeter preceded by a 3, 7 (orange in Figure 8), or 14-day (red in Figure 8) interval that included rainfall. Previous work on the relationship between rainfall and creep events have found that creep events that are associated with rainfall tend to occur within 24 hr of rainfall (Roeloffs, 2001; Schulz et al., 1983). The range of thresholds we used is longer than this to allow for varying timescales of rain infiltration as this is not a well-known quantity. Although fairly arbitrary, these timescales provide an ability to look at the broad overview of the effect of rainfall on the propagation of creep events within our statistical framework. Despite not being an in-depth analysis of this topic, we believe these timescales are sufficient to interpret our findings in the light of rainfall.

Events with rainfall before them were then removed from the main creepmeter before bootstrapping (Figure 8a) and shifting (Figure 8b) of the creep event data set at the main creepmeter. We then computed the subtraction as before to determine the percentage of physically related creep events in the following wet and dry periods (Figure 8c).

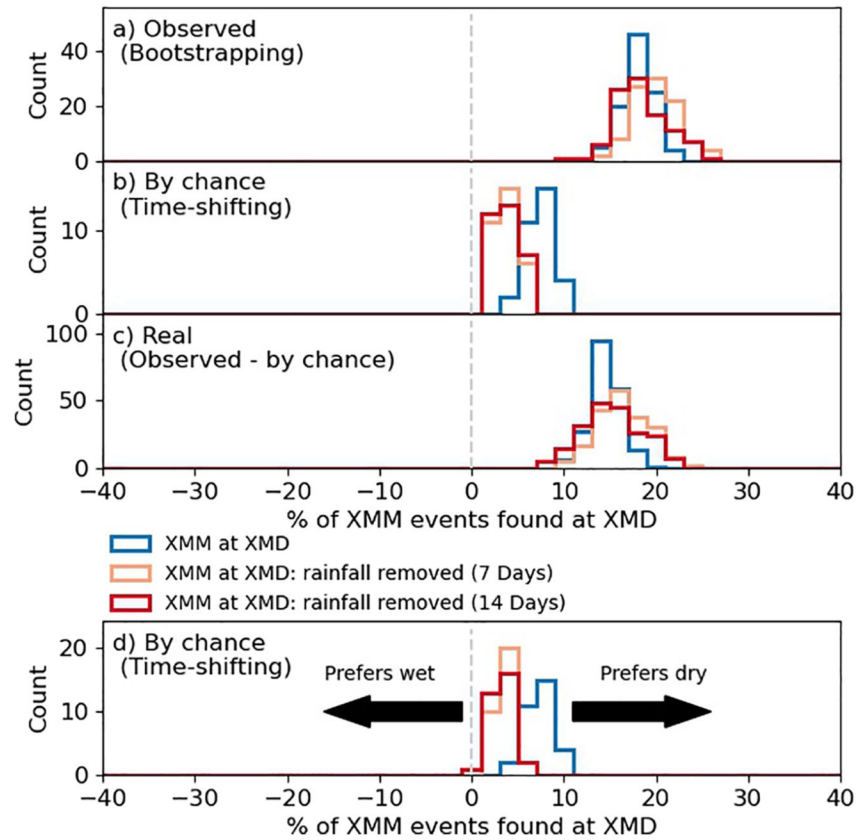


**Figure 8.** (a)–(c) Probability distributions on the percentage of Middle Mountain (XMM) events observed at Middle Ridge (XMD). Panels a–c are as in Figure 7, with the observed, by chance, and real percentages, but the three histograms in each panel illustrate the effect of removing rainy intervals. The blue histograms use all XMM events in the comparison while the orange and red histograms use only XMM events that follow 7- or 14-day periods without rain. (d) The percentage of XMM events observed at XMD by chance, as in panel b, but when XMD events preceded by rainfall are removed. The reduced percentage suggests that XMD events are more common in rainy intervals.

In this reanalysis, we do not use all creepmeter pairs. We consider only pairs that showed significant correlation to one another before rainfall considerations. If both creepmeters in the pair are triggered by rainfall, we would expect to see a reduction in correlation when we remove events that follow rainfall. Often, however, we see a minimal change in the correlation. For instance, the similarity of the blue to red histograms in Figure 8c suggests that the closely timed creep events at XMM and XMD are caused by something other than rainfall.

We summarize how excluding rainy intervals influences or does not influence the percentage of closely timed creep events for more pairs of creepmeters in Section 5. Those quantified influences are enough to determine the significance or lack of significance in the closely timed event percentages. Here, however, we also briefly consider how rainfall influences creep event timing. To slightly better understand the influence of short-timescale rainfall, we probed the number of creep events at “random” times at the second creepmeter (Figure 8d). To preserve the seasonality, we created random times by shifting the times of the main creepmeter events by multiples of a year. We then excluded events preceded by 3-, 7-, or 14-day intervals with rainfall before computing the percentage of times within 24 hr of a creep event at the second creepmeter (Figure 8d). These new time-shifted distributions allowed us to determine if certain creepmeters preferred to slip in wet or dry conditions (given the seasonality of the main creepmeter). For instance, it appears from Figure 8d that the creepmeter at Middle Ridge (XMD) prefers to slip in wet conditions; the percentage of times with creep events decreases when rainy intervals are removed. We do not discuss this further, however the relevant results are presented in the supplement (Figures S26–S32 in Supporting Information S1).

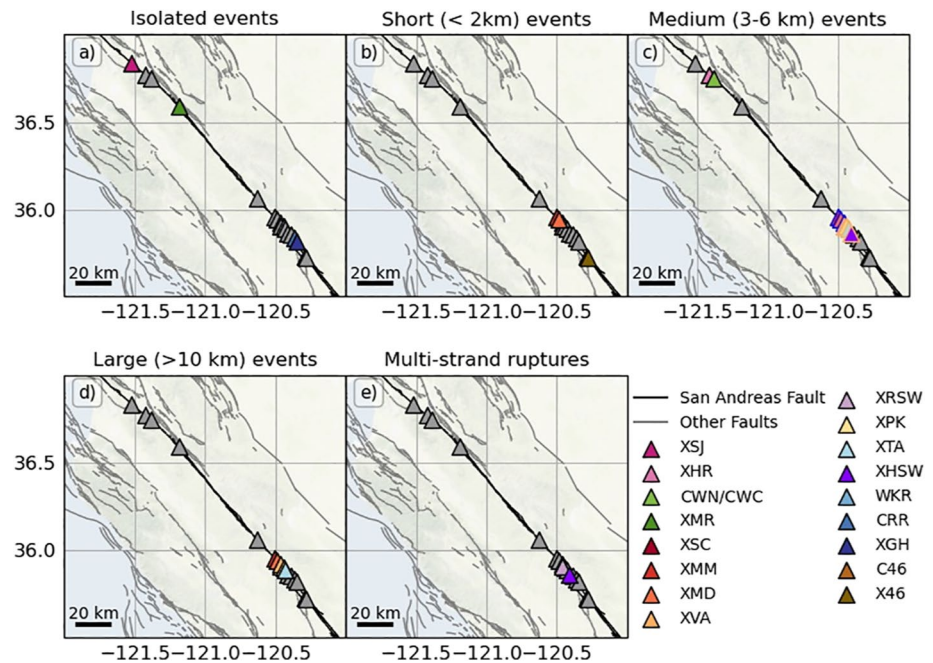


**Figure 9.** Maps of the creeping section of the central San Andreas Fault (black) showing the location of different creep event behaviors. The creepmeters are shown as colored triangles, grayed out triangles are creepmeters not involved in events. (a) Location of isolated events. (b) Location of (<2 km) events recorded at two creepmeters. (c) Location of 5-km events recorded at multiple creepmeters. (d) Location of long (10–30 km) propagating events. (e) Location of multi-strand ruptures.

### 4.3. Detecting Long Creep Events by Visual Inspection

Having determined the frequency of multi-creepmeter events and assessed the effects of rainfall, we next use our event detections to inspect coincidentally timed creep events at multiple creepmeters visually. Using our creep event catalog, we identify all the creep events at each creepmeter that occur within 24 hr of a creep event at any other creepmeter to produce a subsection of our catalog that only contains these events. This subsection of events contains 306 potentially large creep events that rupture two or more creepmeters within 24 hr, made up of 719 different individual detections from our creep event catalog. We present examples of different sized creep events in Section 5 and provide figures illustrating all of the multi-creepmeter events in the second supplementary creep booklet.

Visual inspection also allowed us to probe where slip happens in a creep events: on the surface or at depth. If a creep event was rupturing along the surface we would expect to observe an event at every creepmeter along the way between two end-member creepmeters. However, we do not always find this to be the case which would suggest that these creep events are rupturing at some depth below the surface (Evans et al., 1981). Examples of these events are discussed in Section 5.4.

## 5. Summary of Creep Event Behaviors

The creep event correlation described above reveals that many creep events rupture several kilometers along the fault strike. But other creep events appear short, perhaps less than 1 km long. By analyzing over 2,000 creep events found in our catalog, we are able to identify a variety of creep event behaviors. Here, we describe the five most common creep event types: (a) isolated events (Figure 9a), (b) small (<2 km) events recorded at two creepmeters (Figure 9b), (c) 5-km events recorded at multiple creepmeters (Figure 9c), (d) long (10–30-km) propagating events (Figure 9d), and (e) multi-strand ruptures.

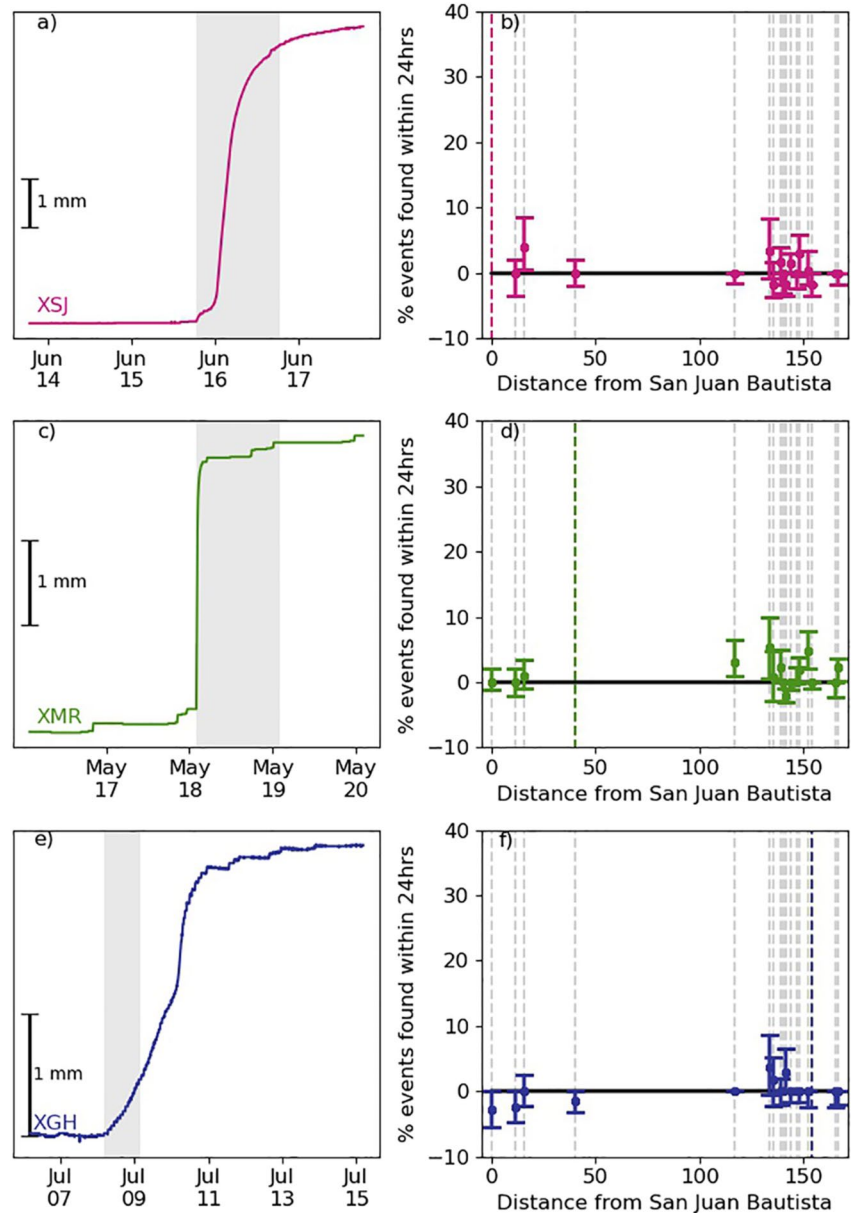


**Figure 10.** Creep events and percentage of events observed at other creepmeters for isolated creep events at San Juan Bautista (XSJ), Melendy Ranch (XMR), and Gold Hill (XGH). (a) Creep event at XSJ on 15 June 1993. (c) Creep event at XMR on 18 May 1993. (e) Creep event at XGH on 8 July 1991. (b), (d) and (f) indicate the percentage of events XSJ, XMR, and XGH events found at other creepmeters, with 70% confidence intervals. Vertical colored lines in (b), (d), and (f) mark the location of the creepmeter.

### 5.1. Isolated Events

A few creepmeters in this study appear to show only isolated creep events: events that are recorded at no other creepmeters. The area of these locations are shown in Figure 9a.

#### 5.1.1. San Juan Bautista (XSJ)

The creepmeter at XSJ displays isolated, repetitive 3- to 4-mm events every few months, which were previously analyzed by Gladwin et al. (1994). One of these isolated events is shown in Figure 10a. The XSJ events show weak to minimal correlation in timing with the closest neighboring creepmeters. Although 0.5%–8.5% of XSJ

events are recorded at CWN 15.3 km southeast according to 70% confidence intervals, 70% confidence intervals overlap zero and have a maximum of 2.0% for a closer creepmeter located 11.2 km southeast (Figure 10b).

### 5.1.2. Melendy Ranch (XMR)

The creepmeter at XMR displays 2-mm events (Figure 10c) every few months that are recorded at no other creepmeter (Figure 10d). However, this creepmeter is far from its neighbors: 24.6 km southeast of CWN and 77.32 km northwest of XSC. Nevertheless, it is interesting to note that this creepmeter is situated above a locked patch identified by Jolivet et al. (2015). The locked patch could prevent creep events from rupturing into and out of the XMR area.

### 5.1.3. Gold Hill (XGH)

The creepmeter at XGH also displays isolated events (Figure 10e). These events are more intriguing than those at XSJ and XMR because XGH is just 2.2 km southeast of the Carr Ranch (CRR) creepmeter, yet there is no evidence of creep events that rupture both locations (Figure 10f). Indeed, on timescales of months to years, these locations seem to have anticorrelated slip rates. For instance, when the slip rate at CRR increased in September 1994, the slip rate at XGH decreased. Moreover, when the slip rate at CRR decreased between 2016 and 2017, the slip rate at XGH increased. This anti-correlation in slip was noted by Roeloffs (2001), who suggested that slip accumulates at one location before reaching a threshold that allows slip at the other location.

## 5.2. Small Events (2 km or Less) Recorded at Two Creepmeters

Some creepmeters record events that coincide in time with events at creepmeter a short distance away. The area of these locations are shown in Figure 9b.

### 5.2.1. Middle Mountain (XMM)–Middle Ridge (XMD)

The fault section between XMM and XMD is around 8 km north of Parkfield. These two creepmeters are 2.26 km from each other, 14.2 km from creepmeters farther north, and 2 km from creepmeters farther south. Both creepmeters record large numbers of <1-mm creep events, which occur every few weeks (see Figure 5a). Our analysis of coincidentally timed events implies that many of these small creep events rupture both creepmeter locations (Figure 11a). 70% confidence intervals suggest that 12.9%–16.3% of XMM events are also recorded at XMD, and 25.9%–31.9% of XMD events are observed at XMM (Figure 11b).

When creep events with rainfall in the 7–14 days before the event are removed, the percentage of XMM events found at XMD and vice versa does not change significantly. When events preceded by a 14-day interval with rainfall are removed, 11.8%–19.0% of XMM events are observed at XMD, and 24.4%–34.7% of XMD events are observed at XMM. Combining these percentages with the observation that XMM and XMD have opposite responses to rainfall (Figure S26g and S26h in Supporting Information S1) implies that correlated events recorded at these two creepmeters are not due to atmospheric effects; instead, their correlation is due to a slip at depth on the fault.

### 5.2.2. Highway 46 Creepmeters (C46–X46)

The southernmost pair of creepmeters is situated near Highway 46, 10 km south of the cluster of creepmeters around Parkfield. Creepmeters C46 and X46 are 1.27 km apart and record fewer events than XMM and XMD; 0.4–1.6-mm events occur around 1–2 times a year. However, many of the recorded creep events rupture both locations (Figure 11c). 70% confidence intervals suggest 50.0%–66.7% of creep events at C46 are observed at X46%, and 47.1%–64.8% of X46 events are observed at C46 (Figure 11d).

When creep events with rainfall in the 7–14 days before the event are removed, the percentage of C46 events at X46 increases. When events with rainfall in the 14 days prior are removed, 40%–80% of C46 events are found at X46, and 100% of X46 events are found at C46 (Figure S27 in Supporting Information S1), which may arise from slip at depth. The picture of this section is not fully clear as both C46 and X46 prefer to slip in wet conditions (Figure S27g and S27h in Supporting Information S1). This would suggest that some of the correlation here is rainfall induced, however, there is still some evidence for slip at depth, given the percentage of correlated events goes up when rainfall is removed.

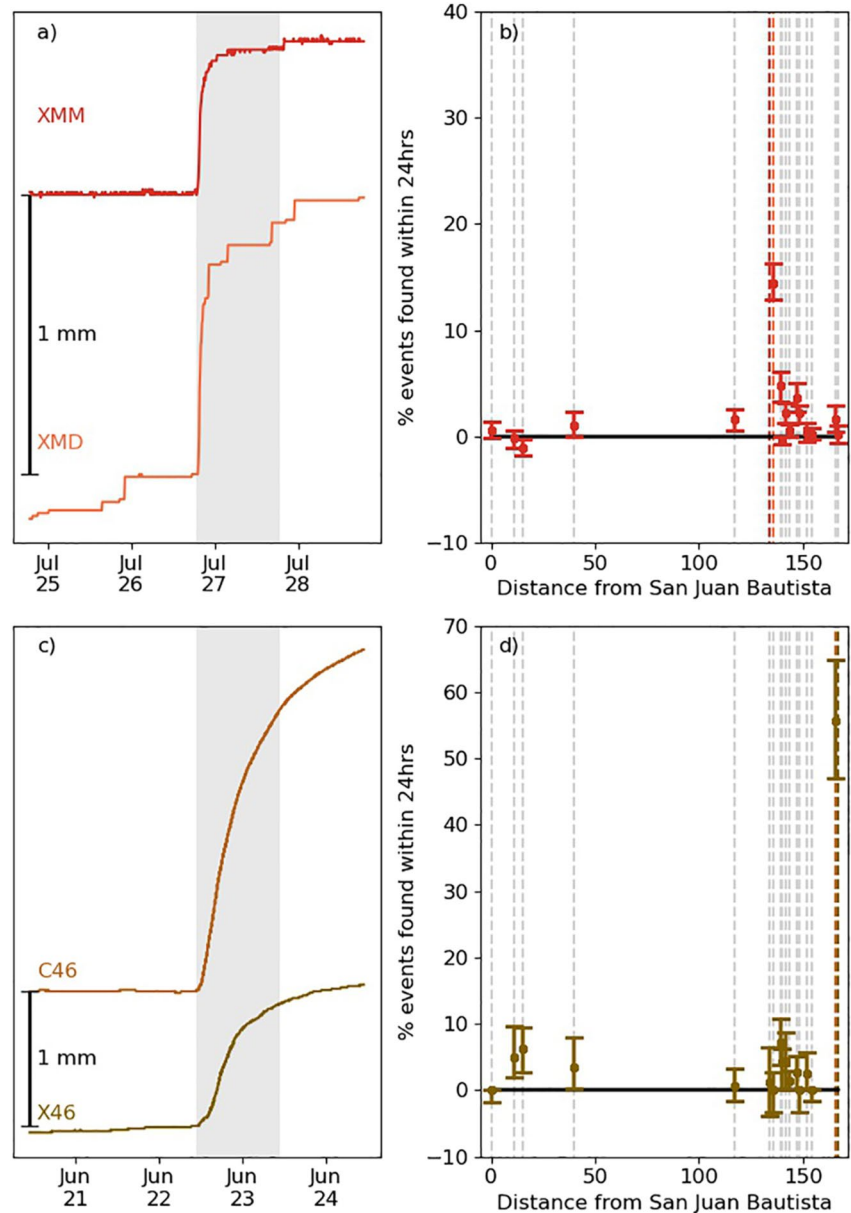


**Figure 11.** Small creep events from the Middle Mountain (XMM)–Middle Ridge (XMD) and Highway 46 (X46 & C46) areas and percentage of events observed at other creepmeters for XMM and X46. (a) Creep event at XMM and XMD on 26 July 1991. (c) Creep event at X46 and C46 on 22 June 2015. (b and d) indicate the percentage of XMM and X46 events found at other creepmeters, with 70% confidence intervals. Vertical colored lines in (b and d) mark the location of the creepmeters in (a and c).

### 5.3. Medium-Sized Events (3–6 km) Recorded at Two or Three Creepmeters

The next most frequently observed type of creep events are 3–6 km long and are typically observed at two or three creepmeters. These 5-km-long events are found at multiple locations along the fault from CWN in the north to Highway 46 in the south. The area of these locations area shown in Figure 9c.

#### 5.3.1. Harris Ranch (XHR)–Cienega Winery (CWN)

The northern end of the creeping section between XHR and CWN hosts a series of creep events that have an along-strike length of at least 4 km (Figure 12a). Events at CWN and XHR are typically 2–2.5 mm and occur

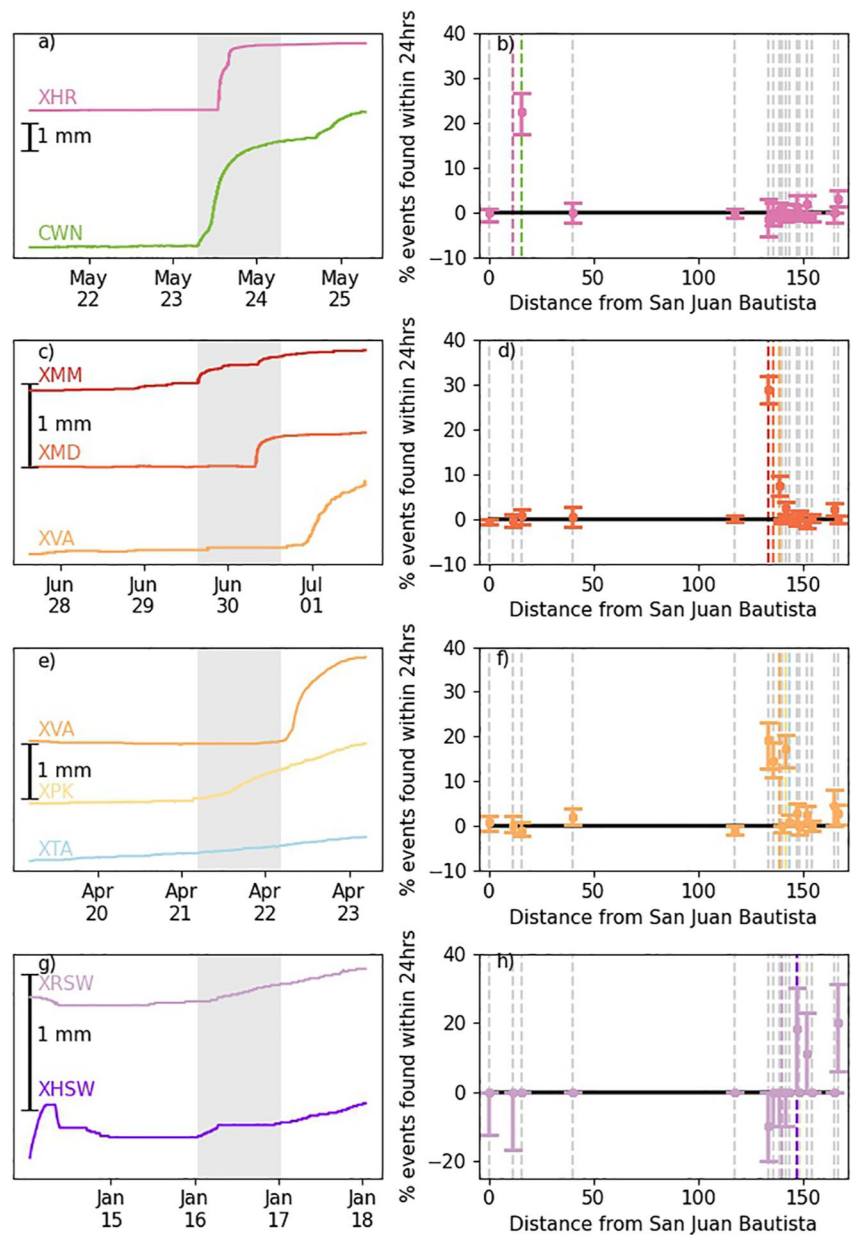


**Figure 12.** Medium-sized creep events from the Harris Ranch (XHR)–Cienega Winery (CWN), Middle Mountain (XMM)–Varian (XVA), XVA–Taylor Ranch (XTA) areas and the Southwest trace [Roberson Southwest (XRSW)–Hearst Southwest (XHSW)] and percentage of events observed at other creepmeters for XHR, Middle Ridge (XMD), XVA, and XRSW. (a) Creep event at XHR and CWN on 11 and 12 February 1994. (c) Creep event at XMM, XMD, and XVA on 29 and 30 June 2014. (e) Creep event at XVA, Parkfield (XPK), and XTA on 21 and 22 April 2008. (g) Creep event at XRSW and XHSW on 16 January 1993. (b, d, f, and h) indicate the percentage of XHR, XMD, XVA, and XRSW events found at other creepmeters, with 70% confidence intervals. Vertical colored lines in (b, d, f, and h) mark the location of the creepmeters in (a, c, e, and g), respectively.

every few months. 70% confidence intervals suggest that 17.4%–26.6% of creep events recorded at XHR are also recorded at CWN, and 21.3%–39.1% of CWN events are observed at XHR (Figure 12b).

When creep events with rainfall in the 7 days before the event are removed, the percentage of XHR events observed at CWN and vice versa does not change significantly, with 16.3%–28.5% of XHR events recorded at CWN and 20.8%–32.0% of CWN events observed at XHR. And if creep events with rainfall in the previous 14 days are excluding, the percentage of events rupturing both stations actually increases. If events with rainfall in the 14 days

before the event are removed, 29.6%–47.6% of XHR events are observed at CWN, and 28.0%–48.7% of CWN events are observed at XHR (Figure S28 in Supporting Information S1). The relationship between XHR, CWN and rainfall is discussed in more detail in Section 6.3.

### 5.3.2. Middle Mountain (XMM)–Middle Ridge (XMD)–Varian (XVA)

Farther south, the fault section between XMM and Varian (XVA) also hosts 5-km-long events. As noted in Section 5.2.1, creep events rupture between XMM and XMD frequently. However, not all of the events in this fault section are simple, 2-km ruptures. Some events continue rupturing farther south to reach XVA (Figure 12c). 70% confidence intervals suggest that XVA events coincide with events at both XMM and XMD. 3.3%–6.1% of events at XMM are observed at XVA, and 12.9%–23.3% of XVA events are observed at XMM (Figure 12d). Further, 5.3%–9.8% of XMD events are observed at XVA, and 11.0%–18.8% of XVA events are observed at XMD (Figure 12d). Three-creepmeter ruptures can start at any of these stations. However, ruptures are most commonly seen first at XMD; the creep events may preferentially nucleate near XMD (Roeloffs et al., 1989; Rudnicki et al., 1993).

We note, however, that some apparent XMM-XVA or XMD-XVA rupture could arise because coincident creep events are triggered by rainfall. When creep events that are preceded by a 7-day interval that includes rainfall are removed, the percentage of XVA events observed at XMM decreases to 6.6%–21.8%, and the percentage of XMM events observed at XVA decreases to 1.3%–5.1%. The percentage of closely timed XMD-XVA events also decreases. 4.9%–17.5% of XVA events observed at XMD and 3.2%–7.3% of XMD events observed at XVA. When events with rainfall in the 14 days prior are removed, the percentage of XVA events at XMM reduces to 1.0%–16.7%. The percentage of XMM events at XVA becomes 0%–4.4%, implying that they may be unrelated. However, the percentages for XMD and XVA remain roughly constant when 7 or 14 days of rainfall are removed. These reductions in percentages imply that XMM and XVA events may be unrelated when longer term rainfall is considered; however, the relation between XMD and XVA remains. These relations suggest that there are often events that rupture from XMD to XVA (a distance of 3.1 km) but do not always rupture up to XMM and may require atmospheric perturbations to do so.

### 5.3.3. Varian (XVA)–Parkfield (XPK)–Taylor Ranch (XTA)

In the last subsection, we discussed creepmeters that observed creep events to the north of XVA. However, XVA also hosts events that are only observed to the south, at the Parkfield creepmeter (XPK, 2.9 km away) and potentially at the Taylor Ranch creepmeter (XTA, 4.8 km away) (Figure 12e). 70% confidence intervals suggest that between 13.2% and 20.5% of XVA events are observed at XPK, and 15.5%–25.3% of XPK events are observed at XVA (Figure 12f). These numbers imply that many events rupture the 2.9 km from XVA to XPK. Many events also rupture the 1.9 km from XPK to XTA; 70% confidence intervals suggest that 5.1%–10.0% of XPK events are recorded at XTA and that 20.3%–34.9% of XTA events are observed at XPK (Figures S17 and S18 in Supporting Information S1). These percentages are minimally affected by removing times with rainfall.

However, even though XVA-XPK and XPK-XTA events are common, few to zero events rupture the entire 4.8 km from XVA to XTA; 70% confidence intervals suggest that 0%–2.6% of XVA events are found at XTA and that 0%–9.1% of XTA events are found at XVA (Figure 12f). When rainfall is removed, the percentages of XVA events at XTA and vice versa are reduced slightly, with the lower bound remaining at 0%, meaning that the coincidentally timed XVA and XTA events may either be unrelated or driven by rainfall. The lack of closely timed events at XVA and XTA suggests that creep events along this region prefer to slip in two sections: XVA to XPK (2.9 km) or XPK to XTA (1.9 km). Creep events rupture the 4.8 km from XVA to XTA less frequently or perhaps not at all.

### 5.3.4. Roberson Southwest (XRSW)–Hearst Southwest (XHSW)

Medium-sized multi-creepmeter ruptures may also be present on secondary strands of the San Andreas Fault: in a 6.4-km stretch between Roberson Southwest (XRSW) and Hearst Southwest (XHSW). Events on this secondary strand are less frequent than on the main strand, but we still observe closely timed creep events (Figure 12g). 70% confidence intervals suggest that 4.3%–31.2% of XRSW events are observed at XHSW, and 0.0%–10.3% of XHSW events are observed at XRSW (Figure 12h). The statistics are somewhat difficult to interpret because XRSW displays just 11 creep events and that number is reduced by 50% when we remove creep events preceded by rainfall (Figure S25 in Supporting Information S1). So we simply note here that the XHSW-XRSW statistics marginally suggest that several creep events could rupture the 6 km between these creepmeters.

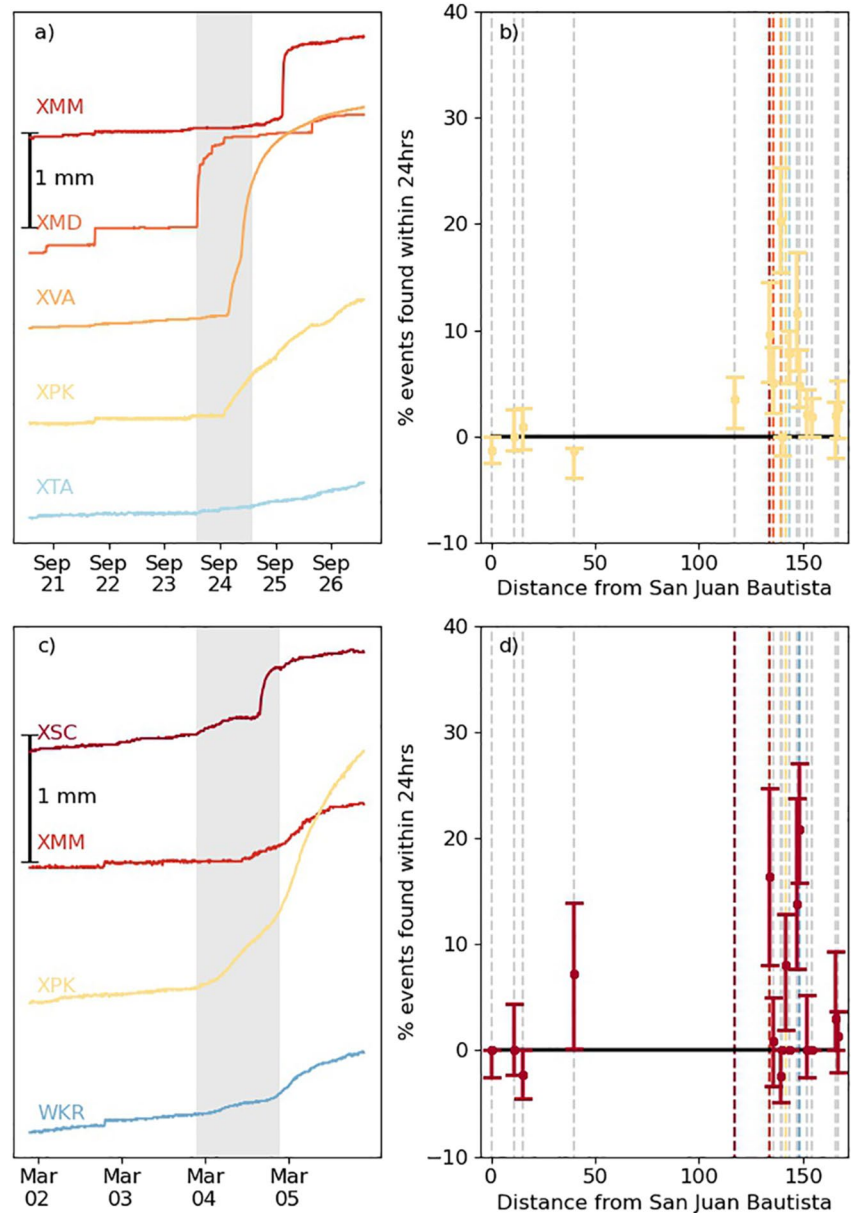


**Figure 13.** Potential large creep events from Slacks Canyon (XSC) to Work Ranch (WKR) section and percentage of events observed at other creepmeters for Parkfield (XPK) and XSC. (a) Creep event on the Middle Mountain (XMM)–Taylor Ranch (XTA) section on 23–25 September 2000. (c) Creep event along the XSC–Work Ranch (WKR) section on 3 and 4 March 1991. (b and d) indicate the percentage of XPK and XSC events found at other creepmeters, with 70% confidence intervals. Vertical colored lines in (b and d) mark the location of the creepmeters in (a and c).

#### 5.4. Large Events (10 km or More), Sometimes Skipping Creepmeters

The potential 6-km creep events between XHSW and XRSW are not the longest creep events we observe. Some closely timed creep events suggest ruptures that span 10 or even 30 km. The area of these locations are shown in Figure 9d.

##### 5.4.1. 10 km Events

The 10-km events occur in the region we discussed in Sections 5.3.2 and 5.3.3, between XMM and Taylor Ranch (XTA), including XMD, XVA, and XPK. Two-creepmeter 2- to 5-km events are frequently observed in this region. But in September 2000, a large creep event was recorded at all five creepmeters (Figure 13a). Such closely

timed slip at these creepmeters seems unlikely to be a coincidence or rainfall-induced; the September event was preceded by 104 days without rainfall. However, we only observe these 10-km XMM to XTA events once suggesting such events are rare; 70% confidence intervals suggest that 0%–1.2% of XMM events are observed at XTA and 0%–15.3% of XTA events are observed at XTA.

The 8.2 km-long XMM to Parkfield (XPK) section ruptures more frequently. 70% confidence intervals for this section suggest that 1.2%–3.1% of XMM events are observed at XPK, and 5.1%–14.6% of XPK events observed at XMM (Figure 13b). However, some of the closely timed events could be induced by rainfall. When creep events with rainfall in the 7 days prior are removed, 0.4%–3.8% of XMM events are observed at XPK, and 3.9%–18.4% of XPK events are observed at XMM. Moreover, if events with rainfall in the 14 days prior are removed, the relationship between XMM and XPK has at least a 15% chance of being explained by atmospheric perturbations.

Assuming that the closely timed slip at XMM and XPK do reflect 8-km-long creep events, it is interesting to note that even when creep events appear to rupture from XMM to XPK, they sometimes do not appear at the creepmeters in the middle (XMD and XVA). The lack of intermediate surface rupture suggests that the creep events commonly rupture at depth and sometimes do not reach the surface.

#### 5.4.2. Potential 31-km Events: Slacks Canyon (XSC)–Work Ranch (WKR)

Some of the largest creep events that we seem to observe are those that propagate between XSC and Work Ranch (WKR), an along-strike distance of 31.2 km. 70% confidence intervals suggest that 15.8%–27.0% of creep events observed at XSC are observed at WKR, and 10.2%–19.6% of WKR events are observed at XSC (Figure 13d). These potentially long events are also observed at some of the creepmeters between them but not at all of the intermediate creepmeters. For instance, in Figure 13c, we have not plotted slip at XMD, XVA, and XTA because they displayed no creep event. Further, the percentage of XSC events observed at XMM and XPK is lower than the percentage of XSC events observed at WKR (Figure 13d).

We note, however, that much of the WKR-XSC correlation could be due to rainfall. If we remove events preceded by a 7-day interval with rainfall, 0.0%–15.5% of XSC events are observed at WKR, and 0.0%–13.0% of WKR events observed at XSC. Those percentages imply a 15% chance that the closely timed events result from hydrological forcing. If events with rainfall in the 14 days prior are removed, there are no closely timed events at XSC and WKR. Further, both XSC and WKR show a strong seasonal signal (Roeloffs, 2001); all of the closely timed creep events between these stations occur between December and March, showing a strong seasonal signal for these long events. Given both XSC and WKR prefer to slip in wet conditions (Figure S29 in Supporting Information S1), one might expect that these potential long events may instead be small local events that occurred at similar times due to atmospheric perturbations and rainfall.

### 5.5. Multi-Strand Ruptures?

The coincidence of creep events on creepmeters separated by 8 km or perhaps even 30 km suggests that widely separated fault locations can communicate with each other on 24-hr timescales. However, the last set of closely timed creep events we examine suggest that creep event slip may spread not just over 8-km distances but also over multiple strands of the San Andreas Fault.

The two instrumented strands of interest are at the southern end of the creeping section, from XVA to CRR. The main San Andreas Fault has creepmeters installed at XVA, Parkfield (XPK), Taylor Ranch (XTA), Work Ranch (WKR), and CRR. The southwest trace has two creepmeters, one at XRSW and another at XHSW. We will focus on correlations with XHSW here because XRSW has too few events to allow robust statistics.

#### 5.5.1. Hearst Southwest (XHSW) and the Main San Andreas Fault Creepmeters

Events at XHSW, on the southwest trace, display several creep events that are coincident with events on the main fault trace. 70% confidence intervals that suggest XHSW events are observed at many different creepmeters: XSC observes 2.7%–13.3% of XHSW events, XMM observed 23.7%–45.2% of XHSW events, XVA observes 0.2%–12.0% of XHSW events, and Parkfield (XPK) observes 11.9%–31.7% of XHSW events; Work Ranch (WKR) observes 13.4%–25.9% of XHSW events; and CRR observes 0.3%–11.4% of XHSW events (Figure 14a).

Some of these percentages decrease to zero when we remove creep events preceded by rainfall. The correlations between XHSW and XVA and XPK could simply reflect a similar preference for slipping in wet conditions

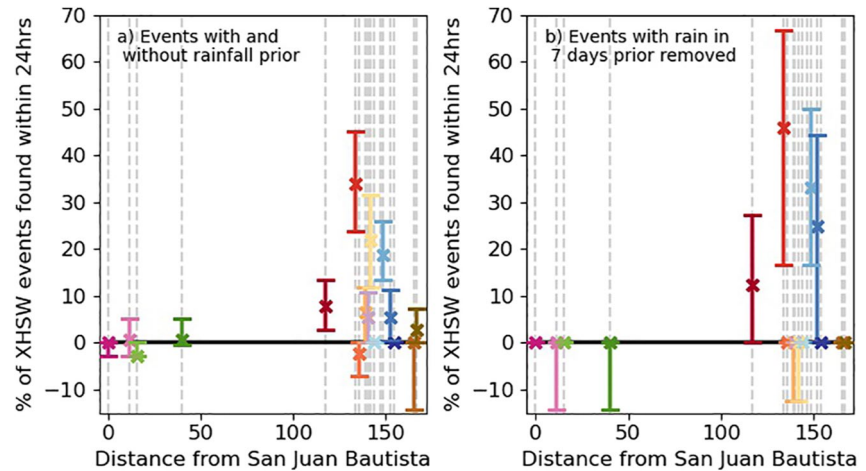


**Figure 14.** Scatter plots of the median percentage of creep events found at Hearst Southwest (XHSW). In panel (a), all XHSW events are included. In panel (b), XHSW events with rainfall in the 7 days prior are removed.

(Figures S31 and S32 in Supporting Information S1). However, other correlations remain even when rainy intervals are removed (Figure 14b). XSC, XMM, WKR, and CRR all show evidence for coincident creep events, with XSC observing 0.0%–27.3% of XHSW events, XMM observing 16.7%–66.7% of XHSW events, WKR observing 16.7%–50.0% of XHSW events, and CRR observing 0.0%–44.4% of XHSW events. Both the XHSW at XSC and XHSW at CRR percentages intersect 0%, suggesting that their relationship may be arising by chance, despite not being driven by rainfall. XMM and WKR still observe a percentage of creep events from XHSW that is significant. WKR and XHSW are 2.12 km apart and are the closest creepmeters from each strand to one another. Their relationship remains even after rainfall effects are considered, this implies that there might be an interaction between the two strands of the San Andreas Fault in this region, which appears to connect at >6 km depth (Waldhauser & Schaff, 2008; N. C. E. D. C., 2014).

## 6. Short-Term Rainfall Influence on Creep Events

The main goal of this study was to catalog creep events to identify creep event behaviors described in Section 5—to determine if creep events routinely rupture several or tens of km along strike. To do so, we examined the percentage of closely timed events at various pairs of creepmeters.

We compared our percentages with those expected for randomly timed creep events in a way that preserved any seasonality in the creep event records. However, creepmeters and creep events can also be triggered by hydrological variations on shorter timescales (Roeloffs, 2001; Schulz, 1989). To assess whether the closely timed events observed at relatively distant creepmeters come from long along-strike ruptures or from a coincident response to rainfall, we redid our analysis after excluding creep events preceded by 3-, 7-, or 14-day intervals that included rainfall. We summarized the implications of those results for inferring creep event sizes in Section 5. However, a more thorough investigation of rainfall responses could teach us more about creep event behaviors. We do not attempt a thorough investigation here, but we briefly discuss why excluding rainfall could leave inter-creepmeter correlations in creep event timing decreased, unchanged, or increased.

### 6.1. Percentage of Correlated Events Decreases

For some creepmeters pairings, the percentage of closely timed creep decreases when we remove events preceded by rainy intervals. Figure 15a shows this effect for the XSC and WKR pair. Both creepmeters are seasonally modulated, with more events in the winter months (Roeloffs, 2001). When we preserve this seasonality but randomize times on shorter timescales (see Section 4.2), we can assess the local creep events' preference for rainfall, and we find that both creepmeters display more events in wet conditions (Figure S29 in Supporting Information S1).

When two creepmeters have a common response to rainfall, we expect that some closely timed events coincide because they both respond to rainfall, not because a larger creep event connects the creepmeters. By removing

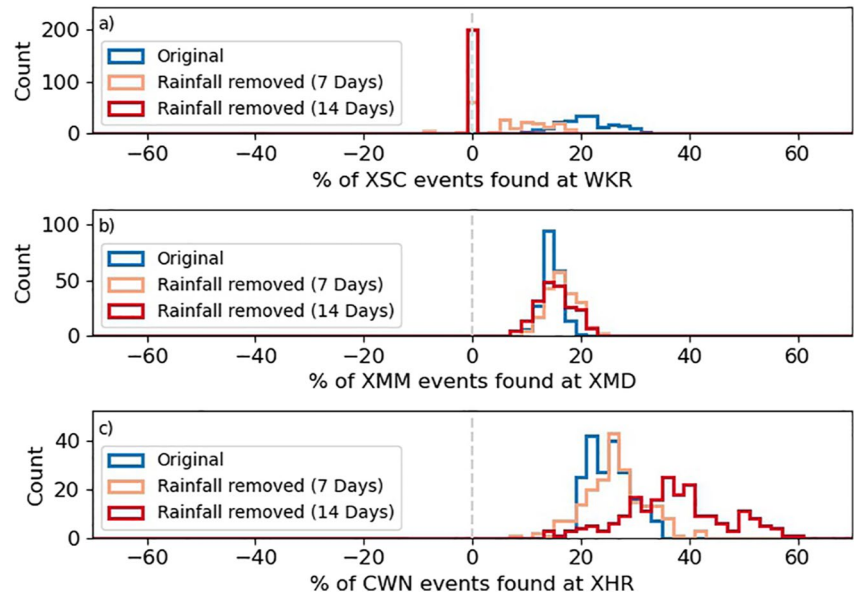


**Figure 15.** Percentage of creep events observed at pairs of creepmeters accounting for rainfall. (a) Percentage of XSC events observed at WKR. (b) Percentage of XMM events observed at XMD. (c) Percentage of CWN events observed at XHR. In (a), (b) and (c) the original percentages are in blue, and the percentage of events after accounting for rainfall in the previous 7 or 14 days are orange and red, respectively.

times preceded by rainfall, we remove the largest-amplitude forcing and expect a reduction in the correlated response. For the XSC-WKR pair, the reduction is significant. When we remove events with rainfall in the 7 days prior, the lower bound of the 70% confidence interval is 0. There is a 15% chance that none of the closely timed creep events reflect spatially expansive creep events. All of them could be coincidental responses to hydrological perturbations.

## 6.2. Percentage of Correlated Events Remains Unchanged

Intriguingly, however, we most commonly find that the percentage of closely timed events remains unchanged when we remove rainy intervals. The median percentage for the XMM-XMD pair, for instance, remains around 14.5%, increasing marginally to 15.9%, as we remove intervals with rainfall (Figure 15b). The lack of change in closely spaced events implies that the creep events respond minimally to short-timescale variations in rainfall or that the responses are uncorrelated at the two creepmeters. While it seems somewhat surprising that short-timescale rainfall responses are commonly uncorrelated between creepmeter locations, it makes many interpretations simple. Since the closely timed creep events are unaffected by rainfall, the correlations must be driven by something else, most likely slip at depth.

## 6.3. Percentage of Correlated Events Increases

However, for one creepmeter pair (XHR-CWN), we find a more dramatic *increase* in the percentage of closely timed events, from 25% to 40%, when we remove events preceded by a 14-day interval that includes rainfall (Figure 15c). The significant percentage change observed when rainfall events are removed from the XHR and CWN events suggests that small single-creepmeter events respond differently to rainfall than larger, multi-creepmeter events. Mortensen et al. (1977) noted that short and shallow creep events occurred at CWN, and longer and deeper creep events would rupture both CWN and XHR. Perhaps the small, shallow events at XHR and CWN are often triggered by rain, and by removing these small events when we remove rainy intervals, we retain only the deeper creep events that span both creepmeters.

## 7. Discussion

We have identified over 2,000 long and short creep events along the San Andreas Fault using cross-correlation, slip thresholding, and manual inspection. The catalog reveals a variety of creep event behaviors. Some creep events are observed only at individual creepmeters, while others appear to rupture to neighboring creepmeters. Most of the multi-creepmeter events appear independent of rainfall; evidence for 2-, 5-, and, 10-km long creep events remains robust when rainfall influences are excluded.

### 7.1. What Drives Creep Events?

Since the discovery of creep events in the 1960s, several mechanisms have been proposed to drive creep events. Here we discuss different models for the driving of creep events and discuss their plausibility in the light of our observed rupture lengths.

Perturbations by rainfall are often thought of as a driving mechanism for creep events, through the close association between rainfall and creep (Roeloffs, 2001; Schulz et al., 1983). Creep events could arise on a stable slip-rate strengthening fault that has been kicked by a rainfall perturbation (Helmstetter & Shaw, 2009; Kanu & Johnson, 2011; Perfettini & Ampuero, 2008). Examples of rainfall triggered events occur at XSC and WKR, both of which are seasonally modulated (Roeloffs, 2001). Most of the kilometer-long events observed, however, appear indifferent to rainfall, with the relationship between some creepmeters even strengthening when rainfall is removed (XHR–CWN). Therefore, it seems hard to explain how small, near-surface stress perturbations would drive creep events that are more than 5 km long. On the other hand, groundwater-driven perturbations could occur later than rainfall, and the fault could accelerate with a time lag, so a lack of timing with rainfall does not exclude this perturbed rate-strengthening model.

Having established that rainfall perturbations are not driving all observed creep events, we must consider other driving mechanisms for creep events. To fully assess these driving mechanisms would require information about the depths that creep events occur which is difficult to determine from creepmeters alone, requiring data from other sources (e.g., strainmeters or tiltmeters). Therefore, we only briefly discuss possible driving mechanisms for creep events and the criteria that our observations provide when assessing these different models.

Given that our observed longer multi-creepmeter events are unlikely to respond to rainfall stress perturbations in the shallow crust, it would seem plausible to consider creep events being driven by frictional weakening of the fault, which drives accelerating albeit aseismic slip. Creep events can be created by patches or layers of slip-rate weakening material that have a particular size: which are large enough to accelerate into creep events but too small to grow into a seismic rupture (Liu & Rice, 2005, 2007; Rubin, 2008; Wei et al., 2013). Such layered rheologies could help explain some of the kinematics and size distribution of creep events (Bilham & Behr, 1992; Bilham et al., 2016; Gladwin et al., 1994), including the tendency of some creep events to skip creepmeters, as observed in events that rupture between XMM and XTA. Such events may rupture continuously at depth but discontinuously along the surface. They may not rupture all surface locations because the fault locally has low stress or a stable rheology (e.g., Luo & Ampuero, 2018).

Models of creep events based on rate weakening patches do have one major issue: tuning. The patches of rate-weakening material must be close enough together to allow aseismic rupture propagation but far enough apart to prevent dynamic rupture (Ando et al., 2010; Luo & Ampuero, 2018; Rubin, 2008; Skarbek et al., 2012; Yabe & Ide, 2017). Our observations provide one more constraint on the patch tuning; creep events must be able to rupture 1-km regions in some instances and to expand 5 or 10 km along strike in other instances.

Given the apparent tuning issues involved in heterogeneity, one might prefer to explain creep events using a different fault zone process: something that promotes initial acceleration but eventually limits slip speeds at a local scale, such as shear-induced fault dilatancy and pore pressure changes (Iverson, 2005; Segall et al., 2010; Segall & Rice, 1995).

Some limited support for dilatancy comes from an indication that pore pressure changes during creep events; the well water level rises or fall during creep events between XMM and XMD (Roeloffs et al., 1989; Rudnicki et al., 1993). However, as rainfall does not trigger or preclude many of our events, dilatancy might not be important to consider as rainfall cannot be providing the pore pressure feedback for dilatant stabilization.

## 7.2. Moment Accommodated by Creep Events?

Though we cannot directly constrain the depth of slip using creepmeter data, the skipped creepmeters noted in Section 7.1, along with the relatively large along-strike extents of some events, suggest that creep events could extend to significant depth—to depths of kilometers to rather than 100 s of meters. And if creep events extend to significant depth, they could have significant moment. Groups of creep events might modulate the moment budget of the San Andreas Fault on decadal or centennial timescales.

Such modulation is interesting to consider because geodetic and repeating earthquake observations have been used to observe variations in the faults' creep rate, with some suggesting this variation occurs on decadal timescales (Khoshmanesh et al., 2015; Khoshmanesh & Shirzaei, 2018a, 2018b; Nadeau & McEvilly, 2004; Sammis et al., 2016; Templeton et al., 2009). Further, large creep events have been reported on the San Andreas Fault and elsewhere (Linde et al., 1996; Martínez-Garzón et al., 2019; Roeloffs, 2001). And a few creepmeters display differently shaped, longer creep events. While most of the creepmeters we examined accumulate 50%–75% of their slip in the small creep events examined here, creepmeters XSC and XTA accumulate only 5%–10% of their slip in small events. Much of the remaining slip accumulates in longer surges of slip, which have an indistinct onset but last weeks to months.

Current geodetic estimates suggest the San Andreas Fault's central creeping section is currently slipping slightly more slowly than its long-term rate. The low slip rate could lead to a  $M_w$  5.2–7.2 earthquake every 150 years (Maurer & Johnson, 2014; Michel et al., 2018; Ryder & Bürgmann, 2008). Alternatively, if creep events play an important role in reducing the creeping region's slip deficit, the low slip rate could lead to a cluster of 30  $M_w$  4 creep events rather than a  $M_w$  5 earthquake. To give that moment context,  $M_w$  4 creep event could be a 4-km long, 4-km deep event with 2 mm of slip. A 4-km long, 1-km deep event with 2 mm would have moment equivalent to a  $M_w$  3.6 earthquake.

We note, of course, that estimating the possible moments of creep events does not tell us whether clusters of tens or hundreds of creep events can occur. To assess the plausible variability of creep events, we would need to better understand the driving physics (Section 7.1). These physics may eventually help us assess whether creeping regions can also rupture in earthquakes and pose a seismic hazard (e.g., Harris, 2017). Many creeping faults appear to be barriers to seismic propagation (e.g., Nocquet et al., 2017; Ryder and Bürgmann, 2008; Thomas et al., 2014; Titus, 2006), but laboratory-based faults often display strong weakening at m/s slip rates, and that dynamic weakening could allow a normally creeping region to rupture in an earthquake (Noda & Lapusta, 2013).

## 8. Conclusion

In this study, we have identified and correlated 2120 creep events recorded on creepmeters along the creeping section of the San Andreas Fault between 1985 and 2020. Some of these creep event detections occur simultaneously at two or more creepmeters; we identify 306 potential events that could rupture multiple creepmeters. Our analysis allows us to identify five groups of creep events: (a) isolated events, (b) small (<2 km) events, (c) medium-sized (3–6 km) events, (d) large events (>10 km), and (e) events that rupture multiple strands. The vast majority of these events are not affected by rainfall. Correlations between creepmeters persist when rainfall influences are excluded. The length of the creep events observed helps us assess the plausibility of different driving models for creep events; local frictional weakening, perhaps with a complex rheology, seems most possible. The creep event lengths, when coupled with the kinematics of slip at various creepmeters, also suggest that creep events rupture both at the surface and at depth. Determining the depth of this slip, and thus of creep events, is an essential next step in understanding the role of creep events in the overall slip dynamics of the creeping section.

## Data Availability Statement

Creep data are provided by the United States Geological Survey and are available at <https://earthquake.usgs.gov/monitoring/deformation/data/download.php>. The plotted fault traces are taken from the Quaternary fault and fold database for the United States, provided by the USGS and the California Geological Survey, and accessed from the USGS website <https://www.usgs.gov/natural-hazards/earthquake-hazards/faults>. Rainfall data are provided by the National Oceanic and Atmospheric Administration and are available at <https://www.ncdc.noaa.gov/cdo-web/datasets>.

### Acknowledgments

Gittins was supported by the Natural Environment Research Council (NERC) Grant NE/S007474/1. We thank Hui Huang for providing insight into fault structure at depth, by examining earthquake locations provided through the Northern California Earthquake Data Center (NCEDC), doi:10.7932/NCEDC. We thank Baptiste Rousset and an anonymous reviewer who helped to improve the content and clarity of this manuscript.

### References

- Ambraseys, N. (1970). Some characteristic features of the Anatolian fault zone. *Tectonophysics*, 9(2–3), 143–165. [https://doi.org/10.1016/0040-1951\(70\)90014-4](https://doi.org/10.1016/0040-1951(70)90014-4)
- Ando, R., Nakata, R., & Hori, T. (2010). A slip pulse model with fault heterogeneity for low-frequency earthquakes and tremor along plate interfaces: Slip pulse model for tremo. *Geophysical Research Letters*, 37. <https://doi.org/10.1029/2010GL043056>
- Bilham, R., & Behr, J. (1992). A two-layer model for aseismic slip on the superstition hills fault, California. *Bulletin of the Seismological Society of America*, 82(3), 1223–1235. <https://doi.org/10.1785/bssa0820031223>
- Bilham, R., & Castillo, B. (2020). The July 2019 Ridgecrest, California, earthquake sequence recorded by creepmeters: Negligible epicentral afterslip and prolonged triggered slip at teleseismic distances. *Seismological Research Letters*, 91(2A), 707–720. <https://doi.org/10.1785/0220190293>
- Bilham, R., Ozener, H., Mencin, D., Dogru, A., Ergintav, S., Cakir, Z., et al. (2016). Surface creep on the North Anatolian Fault at Ismetpasa, Turkey, 1944–2016. *Journal of Geophysical Research: Solid Earth*, 121, 7409–7431. <https://doi.org/10.1002/2016jb013394>
- Bilham, R., Suszek, N., & Pinkney, S. (2004). California creepmeters. *Seismological Research Letters*, 75(4), 481–492. <https://doi.org/10.1785/gssrl.75.4.481>
- Burford, R. O. (1977). Bimodal distribution of creep event amplitudes on the San Andreas fault, California. *Nature*, 268(5619), 424–426. <https://doi.org/10.1038/268424a0>
- N. C. E. D. C. (2014). Northern California earthquake data center. [Data set]. UC Berkeley Seismological Laboratory. <https://doi.org/10.7932/NCEDC>
- Duquesnoy, T., Barrier, E., Kasser, M., Aurelio, M., Gaulon, R., Punongbayan, R. S., & Rangin, C. (1994). Detection of creep along the Philippine Fault: First results of geodetic measurements on Leyte Island, central Philippines. *Geophysical Research Letters*, 21(11), 975–978. <https://doi.org/10.1029/94gl00640>
- Evans, K. F., Burford, R. O., & King, G. C. P. (1981). Propagating episodic creep and the aseismic slip behavior of the Calaveras Fault north of Hollister, California. *Journal of Geophysical Research*, 86(B5), 3721. <https://doi.org/10.1029/JB086B05p03721>
- Fattahi, H., & Amelung, F. (2016). InSAR observations of strain accumulation and fault creep along the Chaman Fault system, Pakistan and Afghanistan. *Geophysical Research Letters*, 43(16), 8399–8406. <https://doi.org/10.1002/2016GL070121>
- Gladwin, M. T., Gwyther, R. L., Hart, R. H. G., & Breckenridge, K. S. (1994). Measurements of the strain field associated with episodic creep events on the San Andreas Fault at San Juan Bautista, California. *Journal of Geophysical Research*, 99(B3), 4559–4565. <https://doi.org/10.1029/93JB02877>
- Gouly, N. R., & Gilman, R. (1978). Repeated creep events on the San Andreas Fault near Parkfield, California, recorded by a strainmeter array. *Journal of geophysical Research*, 83(B11).
- Harris, R. A. (2017). Large earthquakes and creeping faults. *Reviews of Geophysics*, 55(1), 169–198. <https://doi.org/10.1002/2016RG000539>
- Helmstetter, A., & Shaw, B. E. (2009). Afterslip and aftershocks in the rate-and-state friction law. *Journal of geophysical Research: Solid earth*, 114(B1). <https://doi.org/10.1029/2007JB005077>
- Iverson, R. M. (2005). Regulation of landslide motion by dilatancy and pore pressure feedback. *Journal of Geophysical Research*, 110(F2). <https://doi.org/10.1029/2004JF000268>
- Jolivet, R., Lasserre, C., Peltzer, G., Avouac, J.-P., Sun, J., Dailu, R., & Dailu, R. (2013). Spatio-temporal evolution of aseismic slip along the Haiyuan fault, China: Implications for fault frictional properties. *Earth and Planetary Science Letters*, 377–378, 23–33. <https://doi.org/10.1016/j.epsl.2013.07.020>
- Jolivet, R., Simons, M., Agram, P. S., Duputel, Z., & Shen, Z.-K. (2015). Aseismic slip and seismogenic coupling along the central San Andreas Fault. *Geophysical Research Letters*, 42(2), 297–306. <https://doi.org/10.1002/2014GL062222>
- Kaduri, M., Gratier, J.-P., Renard, F., Çakir, Z., & Lasserre, C. (2017). The implications of fault zone transformation on aseismic creep: Example of the North Anatolian Fault, Turkey. *Journal of Geophysical Research: Solid Earth*, 122(6), 4208–4236. <https://doi.org/10.1002/2016JB013803>
- Kanu, C., & Johnson, K. (2011). Arrest and recovery of frictional creep on the southern Hayward fault triggered by the 1989 Loma Prieta, California, earthquake and implications for future earthquakes. *Journal of Geophysical Research*, 116(B4), B04403. <https://doi.org/10.1029/2010JB007927>
- Khoshmanesh, M., & Shirzaei, M. (2018a). Episodic creep events on the San Andreas Fault caused by pore pressure variations. *Nature Geoscience*, 11(8), 610–614. <https://doi.org/10.1038/s41561-018-0160-2>
- Khoshmanesh, M., & Shirzaei, M. (2018b). Multiscale dynamics of aseismic slip on Central San Andreas Fault. *Geophysical Research Letters*, 45(5), 2274–2282. <https://doi.org/10.1002/2018GL077017>
- Khoshmanesh, M., Shirzaei, M., & Nadeau, R. M. (2015). Time-dependent model of aseismic slip on the central San Andreas Fault from InSAR time series and repeating earthquakes. *Journal of Geophysical Research: Solid Earth*, 120(9), 6658–6679. <https://doi.org/10.1002/2015JB012039>
- King, C.-Y. (2019). Kinematics of slow-slip events. In *Earthquakes - Impact, community vulnerability and resilience*. IntechOpen. <https://doi.org/10.5772/intechopen.84904>
- King, C.-Y., Nason, R. D., & Tocher, D. (1973). Kinematics of fault creep. *Philosophical Transactions of the Royal Society of London: Series A, Mathematical and Physical Sciences*, 274, 355–360. Royal Society.
- Langbein, J., Borchardt, R., Dreger, D., Fletcher, J., Hardebeck, J. L., Hellweg, M., et al. (2005). Preliminary report on the 28 September 2004, M 6.0 Parkfield, California earthquake. *Seismological Research Letters*, 76(1), 10–26. <https://doi.org/10.1785/gssrl.76.1.10>
- Langbein, J., & Johnson, H. (1997). Correlated errors in geodetic time series: Implications for time-dependent deformation. *Journal of Geophysical Research*, 102(B1), 591–603. <https://doi.org/10.1029/96JB02945>
- Langbein, J., Quilty, E., & Breckenridge, K. (1993). Sensitivity of crustal deformation instruments to changes in secular rate. *Geophysical Research Letters*, 20(2), 85–88. <https://doi.org/10.1029/92GL02718>
- Lee, J.-C., Angelier, J., Chu, H.-T., Hu, J.-C., & Jeng, F.-S. (2005). Monitoring active fault creep as a tool in seismic hazard mitigation. Insights from creepmeter study at Chihshang, Taiwan. *Comptes Rendus Geoscience*, 337, 1200–1207. <https://doi.org/10.1016/j.crte.2005.04.018>
- Leeman, J. R., Marone, C., & Saffer, D. M. (2018). Frictional Mechanics of slow earthquakes. *Journal of Geophysical Research: Solid Earth*, 123(9), 7931–7949. <https://doi.org/10.1029/2018JB015768>
- Lienkaemper, J. J. (2006). Surface slip associated with the 2004 Parkfield, California, earthquake Measured on alignment arrays. *Bulletin of the Seismological Society of America*, 96(4B), S239–S249. <https://doi.org/10.1785/0120050806>
- Lienkaemper, J. J., McFarland, F. S., Simpson, R. W., Bilham, R. G., Ponce, D. A., Boatwright, J. J., & Caskey, S. J. (2012). Long-term creep rates on the Hayward Fault: Evidence for controls on the size and frequency of large earthquakes. *Bulletin of the Seismological Society of America*, 102(1), 31–41. <https://doi.org/10.1785/0120110033>

- Linde, A. T., Gladwin, M. T., Johnston, M. J. S., Gwyther, R. L., & Bilham, R. G. (1996). A slow earthquake sequence on the San Andreas fault. *Nature*, 383(6595), 65–68. <https://doi.org/10.1038/383065a0>
- Lisowski, M., & Prescott, W. H. (1981). Short-range distance measurements along the San Andreas fault system in central California, 1975 to 1979. *Bulletin of the Seismological Society of America*, 71(5), 1607–1624. <https://doi.org/10.1785/bssa0710051607>
- Liu, Y., & Rice, J. R. (2005). Aseismic slip transients emerge spontaneously in three-dimensional rate and state modeling of subduction earthquake sequences. *Journal of Geophysical Research*, 110(B8). <https://doi.org/10.1029/2004JB003424>
- Liu, Y., & Rice, J. R. (2007). Spontaneous and triggered aseismic deformation transients in a subduction fault model. *Journal Geophysical Research*, 112(B9), B09404. <https://doi.org/10.1029/2007JB004930>
- Luo, Y., & Ampuero, J.-P. (2018). Stability of faults with heterogeneous friction properties and effective normal stress. *Tectonophysics*, 733, 257–272. <https://doi.org/10.1016/j.tecto.2017.11.006>
- Martínez-Garzón, P., Bohnhoff, M., Mencin, D., Kwiatek, G., Dresen, G., Hodgkinson, K., et al. (2019). Slow strain release along the eastern Marmara region offshore Istanbul in conjunction with enhanced local seismic moment release. *Earth and Planetary Science Letters*, 510, 209–218. <https://doi.org/10.1016/j.epsl.2019.01.001>
- Maurer, J., & Johnson, K. (2014). Fault coupling and potential for earthquakes on the creeping section of the central San Andreas Fault: Fault coupling on the creeping SAF. *Journal of Geophysical Research: Solid Earth*, 119(5), 4414–4428. <https://doi.org/10.1002/2013JB010741>
- McHugh, S., & Johnston, M. J. S. (1976). Short-period nonseismic tilt perturbations and their relation to episodic slip on the San Andreas Fault in central California. *Journal of Geophysical Research*, 81(35), 6341–6346. <https://doi.org/10.1029/JB081i035p06341>
- Michel, S., Avouac, J.-P., Jolivet, R., & Wang, L. (2018). Seismic and aseismic moment budget and implication for the seismic potential of the Parkfield segment of the San Andreas Fault. *Bulletin of the Seismological Society of America*, 108(1), 19–38. <https://doi.org/10.1785/0120160290>
- Moore, D. E., & Lockner, D. A. (2013). Chemical controls on fault behavior: Weakening of serpentinite sheared against quartz-bearing rocks and its significance for fault creep in the San Andreas system: Chemical controls on serpentine strength. *Journal of Geophysical Research: Solid Earth*, 118(5), 2558–2570. <https://doi.org/10.1002/jgrb.50140>
- Moore, D. E., & Rymer, M. J. (2007). Talc-bearing serpentinite and the creeping section of the San Andreas fault. *Nature*, 448(7155), 795–797. <https://doi.org/10.1038/nature06064>
- Moore, D. E., & Rymer, M. J. (2012). Correlation of clayey gouge in a surface exposure of serpentinite in the San Andreas fault with gouge from the San Andreas Fault Observatory at Depth (SAFOD). *Journal of Structural Geology*, 38, 51–60. <https://doi.org/10.1016/j.jsg.2011.11.014>
- Mortensen, C. E., Lee, R. C., & Burford, R. O. (1977). Observations of creep-related tilt, strain, and water-level changes on the central San Andreas fault. *Bulletin of the Seismological Society of America*, 67(3), 641–649. <https://doi.org/10.1785/BSSA0670030641>
- Nadeau, R. M., & McEvilly, T. V. (2004). Periodic pulsing of characteristic Microearthquakes on the San Andreas Fault. *Science*, 303(5655), 220–222. <https://doi.org/10.1126/science.1090353>
- Nason, R., & Weertman, J. (1973). A dislocation theory analysis of fault creep events. *Journal of Geophysical Research*, 78(32), 7745–7751. <https://doi.org/10.1029/JB078i032p07745>
- Nocquet, J.-M., Jarrin, P., Vallée, M., Mothes, P. A., Grandin, R., Rolandone, F., & Charvis, P. (2017). Supercycle at the Ecuadorian subduction zone revealed after the 2016 Pedernales earthquake. *Nature Geoscience*, 10(2), 145–149. <https://doi.org/10.1038/ngeo2864>
- Noda, H., & Lapusta, N. (2013). Stable creeping fault segments can become destructive as a result of dynamic weakening. *Nature*, 493(7433), 518–521. <https://doi.org/10.1038/nature11703>
- Perfettini, H., & Ampuero, J.-P. (2008). Dynamics of a velocity strengthening fault region: Implications for slow earthquakes and postseismic slip. *Journal Geophysical Research*, 113(B9), B09411. <https://doi.org/10.1029/2007JB005398>
- Roeloffs, E. A. (2001). Creep rate changes at Parkfield, California 1966–1999: Seasonal, precipitation induced, and tectonic. *Journal of Geophysical Research*, 106(B8), 16525–16547. <https://doi.org/10.1029/2001JB000352>
- Roeloffs, E. A., Burford, S. S., Riley, F. S., & Records, A. W. (1989). Hydrologic effects on water level changes associated with episodic fault creep near Parkfield, California. *Journal of Geophysical Research*, 94(B9), 12387–12402. <https://doi.org/10.1029/JB094iB09p12387>
- Rousset, B., Fu, Y., Bartlow, N., & Bürgmann, R. (2019). Weeks-long and years-long slow slip and tectonic tremor episodes on the South Central Alaska Megathrust. *Journal of Geophysical Research: Solid Earth*, 124(12), 13392–13403. <https://doi.org/10.1029/2019JB018724>
- Rousset, B., Jolivet, R., Simons, M., Lasserre, C., Riel, B., Milillo, P., & Renard, F. (2016). An aseismic slip transient on the North Anatolian Fault. *Geophysical Research Letters*, 43(7), 3254–3262. <https://doi.org/10.1002/2016GL068250>
- Rubin, A. M. (2008). Episodic slow slip events and rate-and-state friction. *Journal of Geophysical Research*, 113(B11), B11414. <https://doi.org/10.1029/2008JB005642>
- Rudnicki, J. W., Yin, J., & Roeloffs, E. A. (1993). Analysis of water level changes induced by fault creep at Parkfield, California. *Journal of Geophysical Research*, 98(B5), 8143–8152. <https://doi.org/10.1029/93JB00354>
- Ryder, I., & Bürgmann, R. (2008). Spatial variations in slip deficit on the central San Andreas Fault from InSAR. *Geophysical Journal International*, 175(3), 837–852. <https://doi.org/10.1111/j.1365-246X.2008.03938.x>
- Sammis, C. G., Smith, S. W., Nadeau, R. M., & Lippoldt, R. (2016). Relating transient seismicity to episodes of deep creep at Parkfield, California. *Bulletin of the Seismological Society of America*, 106(4), 1887–1899. <https://doi.org/10.1785/0120150224>
- Schulz, S. (1989). *Catalog of creepmeter measurements in California from 1966 through 1988*. (U.S. Geological Survey Open File Report No. 89-650).
- Schulz, S., Burford, R. O., & Mavko, B. (1983). Influence of seismicity and rainfall on episodic creep on the San Andreas Fault System in central California. *Journal of Geophysical Research*, 88(B9), 7475–7484. <https://doi.org/10.1029/JB088iB09p07475>
- Segall, P., & Rice, J. R. (1995). Dilatancy, compaction, and slip instability of a fluid-infiltrated fault. *Journal of Geophysical Research*, 100(B11), 22155–22171. <https://doi.org/10.1029/95JB02403>
- Segall, P., Rubin, A. M., Bradley, A. M., & Rice, J. R. (2010). Dilatant strengthening as a mechanism for slow slip events. *Journal of Geophysical Research*, 115(B12), B12305. <https://doi.org/10.1029/2010JB007449>
- Shibazaki, B., & Iio, Y. (2003). On the physical mechanism of silent slip events along the deeper part of the seismogenic zone. *Geophysical Research Letters*, 30(9). <https://doi.org/10.1029/2003GL017047>
- Skarbek, R. M., Rempel, A. W., & Schmidt, D. A. (2012). Geologic heterogeneity can produce aseismic slip transients. *Geophysical Research Letters*, 39(21). <https://doi.org/10.1029/2012GL053762>
- Slater, L. E., & Burford, R. O. (1979). A comparison of long-baseline strain data and fault creep records obtained near Hollister, California. *Tectonophysics*, 52(1), 481–496. [https://doi.org/10.1016/0040-1951\(79\)90263-4](https://doi.org/10.1016/0040-1951(79)90263-4)
- Steinbrugge, K. V., Zacher, E. G., Tocher, D., Whitten, C. A., & Claire, C. N. (1960). Creep on the San Andreas Fault. *Bulletin of the Seismological Society of America*, 50(3), 389–415. <https://doi.org/10.1785/bssa0500030389>
- Templeton, D. C., Nadeau, R. M., & Bürgmann, R. (2009). Distribution of postseismic slip on the Calaveras fault, California, following the 1984 M6.2 Morgan Hill earthquake. *Earth and Planetary Science Letters*, 277(1), 1–8. <https://doi.org/10.1016/j.epsl.2008.09.024>

- Thomas, M. Y., Avouac, J.-P., Champenois, J., Lee, J.-C., & Kuo, L.-C. (2014). Spatiotemporal evolution of seismic and aseismic slip on the Longitudinal Valley Fault, Taiwan. *Journal of Geophysical Research: Solid Earth*, 119(6), 5114–5139. <https://doi.org/10.1002/2013JB010603>
- Titus, S. J. (2006). Thirty-five-year creep rates for the creeping segment of the San Andreas Fault and the effects of the 2004 Parkfield earthquake: Constraints from alignment arrays, continuous global positioning system, and creepmeters. *Bulletin of the Seismological Society of America*, 96(4B), S250–S268. <https://doi.org/10.1785/0120050811>
- Titus, S. J., Dyson, M., DeMets, C., Tikoff, B., Rolandone, F., & Burgmann, R. (2011). Geologic versus geodetic deformation adjacent to the San Andreas fault, central California. *The Geological Society of America Bulletin*, 123(5–6), 794–820. <https://doi.org/10.1130/B30150.1>
- Topozada, T. R., Branum, D. M., Reichle, M. S., & Hallstrom, C. L. (2002). San Andreas Fault Zone, California: M 5.5 earthquake history. *Bulletin of the Seismological Society of America*, 92(7), 2555–2601. <https://doi.org/10.1785/0120000614>
- Waldhauser, F., & Schaff, D. P. (2008). Large-scale relocation of two decades of Northern California seismicity using cross-correlation and double-difference methods. *Journal of Geophysical Research*, 113(B8). <https://doi.org/10.1029/2007JB005479>
- Wei, M., Kaneko, Y., Liu, Y., & McGuire, J. J. (2013). Episodic fault creep events in California controlled by shallow frictional heterogeneity. *Nature Geoscience*, 6(7), 566–570. <https://doi.org/10.1038/ngeo1835>
- Wesson, R. L. (1988). Dynamics of fault creep. *Journal of Geophysical Research*, 93(B8), 8929. <https://doi.org/10.1029/JB093iB08p08929>
- Yabe, S., & Ide, S. (2017). Slip-behavior transitions of a heterogeneous linear fault. *Journal of Geophysical Research: Solid Earth*, 122(1), 387–410. <https://doi.org/10.1002/2016JB013132>